

**GEOCHEMISTRY OF LEACHATE FROM A
NATURALLY WEATHERING DULUTH COMPLEX
ROCK PILE: SULFUR REMOVAL MODELS FOR A 38
YEAR RECORD OF LEACHATE COMPOSITION**

February 2016

Minnesota Department of Natural Resources
Division of Lands and Minerals
500 Lafayette Road, Box 45
Saint Paul, MN 55155-404

**GEOCHEMISTRY OF LEACHATE FROM A
NATURALLY WEATHERING DULUTH COMPLEX
ROCK PILE: SULFUR REMOVAL MODELS FOR A 38
YEAR RECORD OF LEACHATE COMPOSITION**

February 2016

Zach Wenz

Minnesota Department of Natural Resources
Division of Lands and Minerals
500 Lafayette Road, Box 45
Saint Paul, MN 55155-404

TABLE OF CONTENTS

List of Tables	i
List of Figures	ii
List of Appendices	iii
Executive Summary	iv
1.0 Introduction	1
2.0 Rock Weathering Geochemical Principles Summary	1
3.0 Methods	2
3.1 Duluth Complex Leach Pile Construction and Monitoring	2
3.2 Composite Leachate Composition Calculation.....	3
3.3 Solid Phase Analysis.....	3
3.4 Leachate Analysis	4
3.5 Empirical and Theoretical Modeling Approach.....	4
4.0 Results	5
4.1 DCLP Composite Sample Solid Phase Analysis	5
4.1.1 Bulk Sample.....	5
4.1.1 Particle Size Interval Samples.....	5
4.2 DCLP Leachate Composition Trend Analysis.....	6
4.2.1 DCLP Leachate pH and Specific Conductivity	6
4.2.2 DCLP Leachate Sulfate and Major Cation Concentration Trends.....	7
4.2.3 DCLP Leachate Nickel, Copper, Cobalt and Zinc Concentration Trends	7
4.2.4 DCLP Leachate Mineral Saturation Indices	7
4.3 Comparison Between Field and Laboratory Scale Rock Weathering Leachate Trends	7
4.4 Scanning Electron Microscopy Sulfide Grain Size Distribution	8
4.5 Sulfur Release Models	8
4.5.1 Empirical Model	9
4.5.2 Theoretical Model.....	9
4.5.3 Model Comparison.....	11
5.0 Discussion	11
5.1 Model Sensitivity	11
5.2 Model Interpretation	12
6.0 Acknowledgements	14
7.0 References	15

LIST OF TABLES

Table 4.1	Bulk and particle size interval XRD and MLA mineralogy.....	18
Table 4.2	Bulk sample major oxide concentrations.....	19
Table 4.3	Bulk sample and particle size interval total sulfur, carbon, chloride, fluoride, and bromide concentrations.....	20
Table 4.4	Bulk and particle size interval trace metal and nonmetal analyses.....	21
Table 4.5	Mass weighted particle size sieve analysis.....	22
Table 4.6	MLA determined sulfide grain size distribution.....	23
Table 4.7	MLA determined sulfide surface area exposed in wt%.....	24
Table 4.8	Measured sulfate release rates from the Amax field study composite and the DCLP.....	25
Table 4.9	Theoretical model sulfide sphere calculations and parameter values for each of five particle size intervals.....	26
Table 4.10	Theoretical calculation of cumulative mass of sulfur removed.....	27
Table 4.11	Tabulated surface area for 1 gram of pyrrhotite spheres over a range of diameters.....	28

LIST OF FIGURES

Figure 1.1	Surveyed topography of the DCLP and satellite image of the Hibbing field research site indicating the location of the DCLP.....	29
Figure 2.1	Mineral reaction rates as a function of pH.....	30
Figure 3.1	Leachate sulfate concentrations for the three former Amax field study rock piles and the calculated volume weighted composite values used in this study.....	31
Figure 4.1	DCLP 38 year record of leachate sulfate concentration illustrating four principal concentration trends.....	32
Figure 4.2	Leachate pH time series plot for the DCLP.....	33
Figure 4.3	Leachate pH time series plot for the DCLP composite calculation and the three Amax field study rock piles the DCLP was calculated from.....	34
Figure 4.4	DCLP leachate specific conductivity time series plot.....	35
Figure 4.5	DCLP leachate sulfate and major cations concentrations time series plot.....	36
Figure 4.6	Select DCLP leachate metal concentrations time series plot.....	37
Figure 4.7	Sulfate release rate time series plot for leachate from the DCLP and a MN DNR Duluth Complex humidity cell.....	38
Figure 4.8	Empirical model of the linear and power function fit to the measured annual sulfate release rates.....	39
Figure 4.9	Surface area normalized pyrrhotite oxidation rates as a function of pH.....	40
Figure 4.10	Theoretical model cumulative sulfur removal predictions for the normal and greater fines examples.....	41
Figure 4.11	Cumulative sulfide removal of the greater fines example indicating the particle lifetime of the sulfide grains from specific rock particle size intervals.....	42
Figure 4.12	Cumulative sulfur removal plot for the empirical and theoretical models.....	43
Figure 4.13	Relative percent difference of cumulative sulfur removal between the empirical model and the theoretical models.....	44

LIST OF APPENDICES

- Appendix 1 DCLP leachate composition and flow volume data set.
- Appendix 2 DCLP pre-1996 leachate composite calculation data set.

EXECUTIVE SUMMARY

The Minnesota Department of Natural Resources (MN DNR) has been performing environmental research to assess the reactivity of sulfide bearing rock for decades. One of the longest running experiments is the Duluth Complex Leach Pile (DCLP) located at the MN DNR Hibbing field research site. The DCLP is a composite of three sulfide bearing Duluth Complex rock piles originally constructed under a 1978 cooperative research agreement between the MN DNR and Amax Environmental Services Inc. Upon termination of the cooperative research program in 1994, rock from three of the piles was moved to Hibbing to continue the experimental work. At the Hibbing field research site, the rock was placed on a double lined leachate collection system and has been monitored since 1996. The continuation of this rock weathering experiment has documented a 38 year record of a changing rock leachate composition.

The DCLP leachate composition and flow volume data was used to calculate annual sulfate release rates from 1978 to 2015. These release rates are incorporated into an empirical model that numerically describes the rate of sulfur removal from the rock pile over time. This empirical model shows that over the 38 year period of record, the rate of sulfur release has decreased by about a factor of six, and approximately 1,000 kg of sulfur has been removed from the 812 tonne rock pile.

A theoretical model was developed using a shrinking particle model that incorporated rock characterization data (e.g., sulfur concentration, particle size distribution, and sulfide surface area exposed) and an experimentally derived sulfide oxidation rate law. The sensitivity of the theoretical model to the changing mass fractions of different rock particle sizes was investigated. The sensitivity analysis found that the theoretical model is very sensitive to the mass of particles less than about 0.149 mm highlighting that a well-defined particle size distribution is paramount for accurate theoretical predictions.

The theoretical model results are within a factor of two of the empirical modeling results demonstrating theoretical prediction can be a relatively accurate approach when the chemical and physical parameters of the waste rock are well defined. The relatively close agreement between the empirical and theoretical sulfur removal models demonstrates that theoretical approaches for predicting the rate of sulfur removal from a waste rock can be of value for developing mine waste management strategies.

1.0 INTRODUCTION

The Minnesota Department of Natural Resources (MN DNR) has conducted numerous field and laboratory rock weathering experiments. Some of these experiments have operated for long periods of time providing the opportunity to characterize how the governing hydrogeophysical properties change as the reactant mass, namely sulfide minerals, decreases. This report focuses specifically on Duluth Complex waste rock extracted from the Mesaba prospect in the late 1970's. Historically, the Mesaba prospect has been referred to as the Babbitt or Minnamax prospect. This report combines previously reported rock leachate data (Lapakko et al., 2004) with new data to evaluate the long term changes of leachate geochemistry for sulfide-bearing Duluth Complex waste rock. The rock leachate data is used to develop a data based empirical model and compare it to a theoretical model to identify the governing physical and hydrogeochemical parameters.

In 1977, Amax Exploration Inc. constructed six rock piles consisting of lean ore from the Duluth Complex Mesaba prospect (fig. 1.1). The rock piles ranged in mass from 830 to 1700 tonnes and had average sulfur concentrations between 0.6 and 1.4 wt%. In 1978, the MN DNR and Amax Environmental Services Inc. initiated a cooperative environmental research program to evaluate the composition of leachate emanating from the rock piles. Leachate from these rock piles was collected and analyzed until 1994, when the MN DNR and United States Bureau of Mines (USBM) performed a comprehensive characterization study of the rock piles during reclamation of the site. The leachate monitoring and subsequent MN DNR and USBM characterization study are collectively referred to as the 'Amax field study' (reported in Eger et al., 1979; Eger and Lapakko, 1985; and Lapakko et al., 2004). During the reclamation process, some rock from three of the piles was extracted, temporarily stored under cover, and ultimately placed on a leachate collection system at the MN DNR Hibbing field research site in 1996. The composite of the material from the three Amax field study rock piles is referred to as the Duluth Complex Leach Pile (DCLP) and has a volume weighted average sulfur concentration of 0.91 wt%. The DCLP was originally constructed to generate leachate for assessment and developing treatment methods for metal-rich acidic leachate. Beginning in 1996, leachate from the DCLP has been monitored and treated at the MN DNR Hibbing field research site (fig. 1.1). Collectively, the Amax field study and monitoring of the DCLP represent a 38 year record of the leachate composition from naturally weathering sulfide bearing Duluth Complex waste rock.

The objective of this report is to use the 38 year DCLP dataset to evaluate the changing composition of the rock leachate and develop an empirical model to describe the rate at which sulfur is removed from the rock pile. This empirical model is then compared to a theoretical model to identify the governing physical and hydrogeochemical factors and how they have changed over time. Substantiating a theoretical model for predicting long term solute release would provide a valuable predictive tool that can be used by the MN DNR to more accurately execute environmental review and mine permitting responsibilities. Of particular importance is identifying an accurate method for determining long term mining impacts which can be used to inform mine waste management strategies for existing and proposed mining operations.

2.0 ROCK WEATHERING GEOCHEMICAL PRINCIPLES SUMMARY

Mineral reaction rates, such as sulfide oxidation, are fundamentally dependent on the amount of surface area available for reaction (eq. 2.1). As mineral surface area increases, the rate of reaction increases resulting in a greater production of reactants per unit time.

$$r = A_{SA} \times k_+ \qquad \text{eq. 2.1}$$

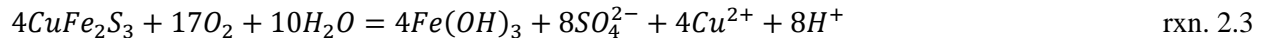
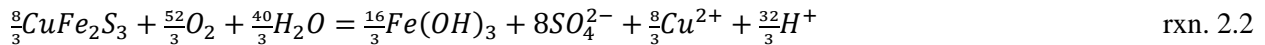
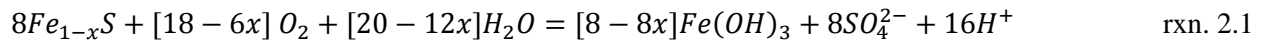
r = rate of reaction ($\text{mol}\cdot\text{sec}^{-1}$)

A_{SA} = surface area (m^2)

k_+ = dissolution flux or 'rate constant' ($\text{mol}\cdot\text{m}^{-2}\cdot\text{s}^{-1}$)

Numerous researchers have determined that sulfide oxidation rates are also dependent on fluid pH and the concentration of the oxidant (McKibben and Barnes, 1986; Williamson and Rimstidt, 1994; Holmes and Crundwell, 2000; Kimball et al., 2010; and Bilenker et al., 2015). Silicate mineral reaction rates are also commonly dependent on fluid pH, but generally have much slower reaction rates. Carbonate minerals reaction rates are strongly dependent on fluid pH and have reaction rates similar in magnitude or greater than many sulfide oxidation rates. Figure 2.1 illustrates the relative rates of reaction for some minerals common in Duluth Complex rock types.

For a naturally weathering waste rock pile it is the complex interplay of the various physical and hydrogeochemical processes that ultimately lead to the leachate concentration. For Duluth Complex rock, water and oxygen contacting the sulfide minerals pyrrhotite (Fe_{1-x}S), cubanite (CuFe_2S_3), and chalcopyrite (CuFeS_2) will generate acid (H^+) through oxidation reactions (rxns 2.1-2.3). The acid generated by these reactions can be neutralized by alkalinity generated from reaction of carbonate and silicate minerals such as calcite (CaCO_3) and plagioclase ($\text{CaAl}_2\text{Si}_2\text{O}_8$, anorthite end member) via reactions 2.4 and 2.5, respectively. The final pH of the leachate depends on the relative amounts of surface area reacted from each of the minerals and the dissolution flux (k_+) of each reaction. As the amount of sulfide surface area increases relative to the neutralizing minerals the leachate pH will decrease. Olivine and plagioclase are much more reactive in weakly acidic fluids (fig 2.1) than many other silicates. The Duluth Complex typically contains low concentrations of carbonate minerals with wt% CaCO_3 concentrations commonly less than 0.2 (Lapakko et al., 2013; Wenz et al., 2013; and Kellogg et al., 2014). This small amount of carbonate is important for neutralizing acid early in the lifetime of a weathering rock pile, particularly for rock with a low sulfide concentration. After the neutralization provided by carbonate minerals is depleted, the abundant silicate mineral assemblage becomes the most important acid neutralizer. The Duluth Complex is generally troctolitic to gabbroic in composition, thus the mineralogy is predominantly olivine ($(\text{Fe},\text{Mg})_2\text{SiO}_4$) and plagioclase ($(\text{Ca},\text{Na})(\text{Al},\text{Si})_4\text{O}_8$). Therefore, the silicate mineral assemblage of Duluth Complex rock types can provide a substantial amount of neutralization despite containing a small amount of carbonate.



3.0 METHODS

3.1 Duluth Complex Leach Pile Construction and Monitoring

In 1994, the Amax field study located near Babbitt Minnesota was deconstructed and reclaimed. Of the six original Amax field study rock piles, rock from three of the piles was extracted and transported to Hibbing Minnesota. At the MN DNR Hibbing field research site the rock was temporarily stored in a 30

mil chlorosulfonated polyethylene (CSPE) synthetic rubber cover and liner system until a leachate collection system and water treatment plant was built. The leachate collection system consists of a double-lined containment system with a drain for collection of the leachate with an underlying leak detection layer. The double-lined system consists of an upper 45 mil CSPE liner underlain by a bed of sand and a 30 mil poly(vinyl chloride) bottom liner. In 1996, construction of the leachate collection system and treatment plant was completed and the temporarily stored rock was placed on the leachate collection system. The leachate emanating from the rock pile flows into a top drain and down through a drain pipe into the treatment plant where the water collects in a bin for a composite sample. When the collection bin is close to filling, a float trigger activates a pump and discharges the water from the bin. The volume of the discharge is recorded by a flow meter.

The rock moved to the Hibbing field research site included the FL1, FL5 and FL6 Amax field study rock piles with estimated volumes of 197, 182, and 289 y³, respectively (Lapakko et al., 2004). The FL1 and FL6 rock piles were uncovered and naturally weathering whereas the FL5 rock pile was covered with a sandy till (30 cm thick in 1980) over coarse sand (about 24 cm thick in May of 1978). The FL5 rock pile was also vegetated and fertilized in 1978 (see Lapakko, 1993 for more details). It is not clear if the cover material on the FL5 pile resulted in a decrease in sulfur removal. Data from the Amax field study indicates that the amount of sulfate released from the rock piles generally increased in the order FL1 > FL6 > FL5, which is consistent with increasing rock pile sulfur concentration. Thus, the cover materials did not result in depressing the sulfate release rate from FL5 to less than that of the FL6 pile. However, it is not clear if the amount of sulfur released from the FL5 pile would have been greater if cover materials had not been applied. In 2015, the DCLP was surveyed using modern GPS survey equipment (fig. 1.1). The 2015 survey found the rock pile volume was 488 y³, which is 180 y³ less than the original estimate. Calculations for this study used the 488 y³ volume for the DCLP, an estimated rock pile porosity of 25%, and a rock density of 3.0 g/cm³, which corresponds to a rock pile mass of 812,146 kg.

From 1996 to 2002, leachate from the DCLP was collected and analyzed intermittently during the spring to fall months. Beginning in the fall of 2013, leachate collection and analysis resumed. Leachate volume was recorded from 1996 to 1998, 2002, and for some periods in 2013 and 2015. The leachate samples were vacuum filtered through a 0.45 micrometer filter and metal samples were treated with 0.1 mL of analytical grade nitric acid per 50 mL of leachate. Appendix 1 contains all of the DCLP monitoring data.

3.2 Composite Leachate Composition Calculation

An estimate of the pre-1996 DCLP leachate composition was calculated from the FL1, FL5, and FL6 rock pile leachate data set from the Amax field study. This composite leachate composition was based on the volume weighted proportion of each of the three rock piles for which there was a coincident leachate sampling date. This approach allowed for an approximation of what the leachate composition would have been for a rock pile with the same composition as the DCLP (0.91 wt% sulfur). Although this approach is an approximation, the calculated composite leachate solute concentrations are consistent with the anticipated solute concentrations based on the DCLP and original Amax field study rock piles sulfur concentration (fig. 3.1). This estimation approach works well for conservative species (sulfate, calcium, magnesium), but is not accurate for non-conservative species such as bicarbonate (i.e., alkalinity) and metals that have low pH sorption edges (e.g., copper and zinc). The leachate composite calculation spans the period from 1978 to 1993 and is tabulated in Appendix 2.

3.3 Solid Phase Analysis

A 13.7 kg composite sample was collected from the DCLP pile in 2014. The composite sample consisted of large rock samples generally greater than 10×10×10 cm. The weathered rind was sawed from each of the samples to ensure a fresh rock sample for solid phase analysis. The composite sample was crushed

following the ASTM D5744-e1 procedure. A split from the total crushed mass was sieved into five separate particle size intervals from which the mass fractions were determined.

The composite sample was analyzed as a bulk sample and as individual size intervals. The bulk sample was analyzed for mineral content, major oxides, sulfur and carbon, and trace metal and non-metals by Activation Laboratories Ltd (Actlabs). Mineral content was determined by x-ray diffraction (XRD) and Scanning Electron Microscopy (SEM) Mineral Liberation Analysis (MLA). The MLA mineral content for the bulk sample was determined from a split that was crushed down to less than 300 μm . Major oxide concentrations were determined by lithium metaborate-tetraborate fusion followed by nitric acid digestion and inductively coupled plasma-mass spectrometry (ICP-MS) and inductively coupled plasma-optical emission spectrometry (ICP-OES) analysis. Sulfur and carbon were analyzed by combustion in an induction furnace. Trace metals were analyzed by ICP-MS after a sodium peroxide fusion. The sodium peroxide fusion technique dissolves all minerals. Mercury was determined by the cold vapor flow injection mercury system (FIMS) method. Bromide and chloride were measured by instrumental neutron activation analysis (INAA). Fluoride was analyzed by an ion-selective electrode (ISE) method after a lithium metaborate-tetraborate fusion followed by nitric acid digestion with an ammonium citrate buffer added.

MLA analysis was also used to determine the individual sulfide minerals grain size distribution and surface area exposure for each of the five particle size sieve intervals. The surface area exposed was determined in 10% gradations by wt% free surface. The 100 wt% exposed sulfide grains represent the so-called 'liberated' fraction.

3.4 Leachate Analysis

Leachate samples were collected from a holding tank. The holding tank has a capacity of about 12 liters. Once the capacity is near full, an electric float is triggered that turns on a pump which removes approximately 80% of the holding tank capacity. Therefore, at any one time the leachate collected from the holding tank represents a leachate composite for each sampling interval. The leachate pH, acidity or alkalinity, and specific conductivity were measured at the MN DNR Hibbing laboratory. Leachate was analyzed for anion and metal concentrations by the Minnesota Department of Agriculture from 1996 to 2012. In 2013, leachate was analyzed by Pace Analytical Services Inc. Starting in 2014, Legend Technical Services Inc. analyzed the leachate samples using EPA methods 6010B and 6020A for cations and EPA method 9056 for anions.

3.5 Empirical and Theoretical Modeling Approach

Sulfate leachate concentration was used to develop an empirical model for the DCLP that numerically describes the rate of sulfur removal with time. The empirical model was constructed with Microsoft Excel software using linear and nonlinear regression analysis of the annual sulfate release rates measured from the DCLP leachate. For years 1978 to 1995, the rock volume weighted average of the annual sulfate release rates from the AMAX field study (Lapakko et al., 2004) was used. For the years after 1995, the annual volume weighted average of the DCLP leachate composition was used. The theoretical model used the volume weighted particle size distribution of the original Amax field study rock piles, MLA determined sulfide surface exposure values, and a laboratory derived surface area normalized pyrrhotite oxidation rate.

4.0 RESULTS

4.1 DCLP Composite Sample Solid Phase Analysis

The DCLP composite sample was analyzed as a bulk sample and as five different particle size intervals. The five particle size intervals were 2.0-6.35 mm, 0.5-2.0 mm, 0.149-0.5 mm, 0.053-0.149 mm, and <0.053 mm.

4.1.1 Bulk Sample

The bulk sample was analyzed for mineralogy, major oxides, sulfur, carbon, and trace metal and nonmetal analysis. Mineralogy is presented on table 4.1, major oxides on table 4.2, carbon, sulfur and halogen concentrations on table 4.3, and trace metals and nonmetal concentrations on table 4.4.

The mineralogy from XRD and MLA analysis was generally in good agreement. The major discrepancies were the apparent detection of amphibole (14.24 wt%) and non-detection of olivine for the MLA, whereas the XRD analysis identified olivine (8.9 wt%), an amorphous phase (12.9 wt%), and no amphibole. It is possible that the amorphous material was compositionally classified as amphibole by the MLA, but did not have a crystalline structure which would explain why no amphibole was detected from the XRD analysis. The occurrence of the amorphous material indicates substantial post crystallization alteration of some primary mineral phase(s). A petrographic analysis is required to accurately determine the original mineral type of the amorphous material. The XRD analysis also identified low concentrations of cordierite, whereas MLA did not detect cordierite. Mineralogical analyses of the same rock presented in Lapakko et al. (2004) indicated 1.6 to 18.4 wt% olivine, <0.1 to 3 wt% cordierite, and no detection of a pure amphibole phase. The presence of cordierite suggests some amount of assimilation of the adjacent pelitic rocks during crystallization. Based on the classification scheme of Miller et al. (2002) the rock type is either an olivine gabbonorite or norite based on the XRD and MLA analyses, respectively.

Major oxide concentrations were consistent with the mafic mineralogy. Total sulfur and carbon concentrations were determined by combustion of two separate splits at two different labs. Total sulfur was additionally analyzed by sodium peroxide fusion followed by ICP-MS. All carbon and sulfur values were in good agreement. The average total carbon and sulfur concentrations were 0.03 wt% and 1.24 wt%, respectively. Both bromide and fluoride were less than the detection limit and chloride had a concentration of 0.04 wt%. Copper and nickel are the most common trace metals with respective concentrations of 6,630 and 1,420 parts per million (ppm).

4.1.1 Particle Size Interval Samples

The particle size interval samples were analyzed individually for mass fraction, mineralogy, major oxides, sulfur, carbon, and trace metal and nonmetal analysis. The particle size interval data is presented on the same tables as that for the bulk analyses. Dry and wet mass weighted particle size data is presented on table 4.5. The particle size intervals were also analyzed by SEM MLA to determine the sulfide grain size distribution and amount of sulfide mineral exposure. The MLA grain size distribution and sulfide mineral exposure data is presented in tables 4.6 and 4.7, respectively.

Particle size interval mass fractions were determined for both dry and wet sieving. For the less than 0.053 mm interval the wet sieve was only 0.1 wt% greater indicating a very small amount of fine material adheres to the larger particles. The two largest size intervals accounted for 85% of the total mass of the sample. Importantly, the relatively large portion of the sample mass consisting of large particles will limit the overall reactivity of mass due to decreasing the samples specific surface area (SSA; cm²/g).

MLA particle size interval mineralogy generally agreed with the bulk mineralogy. The primary exception was the carbonate and sulfide mineral contents which generally increased with decreasing particle size and plagioclase mineral content which generally decreased with decreasing particle size. The particle size dependent mineralogy trends were also apparent in the major oxide and carbon and sulfur compositions. The SiO₂ and CaO wt% values decreased with decreasing particle size, whereas the sulfur and carbon wt% values increased with decreasing particle size. In addition, the copper and nickel concentrations increased with decreasing particle size consistent with an increase of Cu- and Ni-bearing sulfide mineral content with decreasing particle size.

MLA was used to determine the sulfide mineral grain size distribution and the amount of each sulfide mineral that was exposed for each of the five particle size intervals. The sulfide grain size distributions did not vary substantially among the different sulfide types except for the 0.5-2.0 mm size interval for chalcopyrite. The chalcopyrite grain size distribution for the 0.5-2.0 mm size interval ended at about 400 micrometers, whereas the other sulfides were between about 800 and 1,000 micrometers. No one size interval exhibited 100% exposure for any sulfide mineral. Excluding the 0.053-0.149 mm size interval for pentlandite, the two smallest particle size intervals had about 70-80% of the sulfide minerals exposed. Excluding the 0.5-2.0 mm size interval for cubanite, the two largest particle size intervals had less than about 2 wt% exposure. The 0.149-0.5 mm size interval exhibited the greatest variation among the sulfide mineral types, ranging between about 20 to 50 wt% exposure.

4.2 DCLP Leachate Composition Trend Analysis

The 38 year monitoring record for the DCLP illustrates substantial changes of leachate solute concentrations, indicating changing geochemical conditions. In general, there are four principal leachate solute concentration trends easily identifiable from the DCLP leachate sulfate concentration time series data (fig. 4.1). First, leachate concentration increased for about the first five years. Second, after about year five solute concentrations were relatively stable through about year 13. Third, after about year 13 solute concentrations decreased. Fourth, by year 27 leachate concentrations had apparently stabilized at values about ten times lower than the highest concentrations recorded. The gap in data from year 27 to 34 obscures the exact change of the decreasing solute concentrations. However, it does appear that between years 13 and 27, the decrease in concentration was much greater than the interval from years 27 to 38. The single leachate measurement from year 27 (i.e., 2005) suggest the rapid decrease in leachate solute concentrations may have ended around that time. This generalized solute concentration trend indicates a relatively short lived large solute release period followed by a decreasing solute release rate. The following text describes the time series solute concentrations and other measured leachate parameters in greater detail, though the general trend indicated above remains true for most analytes.

4.2.1 DCLP Leachate pH and Specific Conductivity

The DCLP leachate pH trend is complicated by the history of the placement of the rock comprising the DCLP. Initially, leachate pH for the DCLP composite (calculated from the Amax field study data) was circumneutral, though steadily decreasing, for about one year (fig. 4.2). By year two, leachate pH was about five and steadily decreased to about 4.3 by year 15. Leachate pH was again circumneutral for about two years after the DCLP was constructed (fig. 4.2). Whereas the original pH decrease was due to the development of acidic drainage from sulfide oxidation, the initial circumneutral leachate pH for the DCLP was likely resultant from disturbance of the original flow paths and incorporation of new mineral surfaces for neutralization of acid and/or development of more fine neutralizing material from breaking up reaction products during transport and construction of the DCLP. The initial large leachate pH for the DCLP could also be from neutralization of the leachate as it infiltrated through the fresh sand layer of the leachate collection system. The Amax field study FL6 and FL5 rock piles had sulfur concentrations of 0.80 and 1.41 wt%, respectively, and the DCLP has a rock volume weighted sulfur concentration of 0.91

wt%. Based on rock sulfur concentration the leachate pH of the composite should be similar to the FL6 rock pile leachate pH values (fig. 4.3).

Leachate specific conductivity was generally between 2,000 and 4,000 $\mu\text{S}\cdot\text{cm}^{-1}$ for the first 15 years (fig. 4.4). After construction of the DCLP the maximum specific conductivity decreased from about 4,000 to 1,500 $\mu\text{S}\cdot\text{cm}^{-1}$. From years 34 to 38 specific conductivity has varied from 350 to 900 $\mu\text{S}\cdot\text{cm}^{-1}$.

4.2.2 DCLP Leachate Sulfate and Major Cation Concentration Trends

The DCLP leachate sulfate concentrations have ranged from about 200 to 4,000 mg/L (fig. 4.5). Leachate calcium and magnesium concentrations are roughly similar, although for the first two years and since year 15, the leachate calcium was slightly greater than magnesium. Collectively, calcium and magnesium leachate concentrations have ranged from about 20 to 600 mg/L over the period of record. Leachate sodium concentrations were initially as large as calcium, but substantially decreased over the first few years in comparison to calcium and magnesium. Leachate sodium concentrations have exhibited the greatest magnitude of change decreasing from about 500 to 5. Potassium was analyzed much less frequently and has shown the most stable decreasing trend starting at about 30 mg/L and decreasing to about 5 mg/L. For the 38 years of record, the leachate concentration of sulfate, calcium, magnesium, sodium and potassium have decreased by factors of 20, 20, 26, 120, and 10, respectively.

4.2.3 DCLP Leachate Nickel, Copper, Cobalt and Zinc Concentration Trends

For the first 25 years of record, leachate metal concentrations have decreased in order from nickel > copper > cobalt > zinc (fig. 4.6). For this period, nickel and copper concentrations ranged from about 10 to 200 mg/L and 10 to 100 mg/L, respectively, and cobalt and nickel ranged from about 0.5 to 10 mg/L. For years 27 to 38, metal concentrations decreased in the order copper > nickel > zinc > cobalt. For this later period copper concentrations ranged between 10 to 30 mg/L, nickel between 4 to 12 mg/L, and zinc and cobalt between about 0.2 to 1 mg/L.

4.2.4 DCLP Leachate Mineral Saturation Indices

The 2012 and 2014 to 2015 leachate data was evaluated by geochemical modeling to assess the leachate charge imbalance and mineral saturation indices. Geochemical modeling was performed using the Geochemists Workbench software with the packaged MINTEQA2 database. Charge imbalance error ranged from -6% to 5% with an absolute average of 1.9%. Super saturation of many manganese phases indicates that the manganese in solution is metastable and in time would precipitate. The leachate was also supersaturated with respect to silicon oxide phases (such as chalcedony and quartz), aluminum oxide-hydroxide phases (such as gibbsite and diaspore), iron oxide-hydroxide phases (such as ferrihydrite and goethite), and barite. The leachate was under saturated with respect to gypsum exhibiting a $\log(Q/K)$ between -1.0 and -1.7.

4.3 Comparison Between Field and Laboratory Scale Rock Weathering Leachate Trends

Both field and laboratory scale rock weathering experiments exhibit the same overall leachate concentration trend of initially large solute concentrations that decrease over time. However, the period of time over which the concentration changes occur is drastically different, as is the magnitude of the release rate. For example, humidity cell sulfate release rates decrease by a factor of about two in one year, whereas the DCLP sulfate release rate was relatively constant for about 15 years (fig. 4.7). Some of the possible mechanisms for the disparity are likely related to the available reactant load (e.g., sulfate) and accessibility of the reactants to infiltrating water. In the laboratory setting there is a much greater water to rock (W:R) mass ratio, whereas in a field setting the W:R ratio is typically much smaller and is dependent

on precipitation rates. Moreover, the standard humidity cell is completely saturated each week, efficiently removing the reactant load, whereas in a natural setting infiltrating water likely follows preferred channels except for large precipitation events. This flow channelization phenomenon has been supported by modeling exercises which show infiltration in a field setting develops channelized flow paths that slowly expand over time (Fala et al., 2005). Therefore, field rock weathering experiments exhibit a slower depletion of the available reactant load albeit at a greater leachate concentration (due mainly to the W:R ratio) than laboratory experiments.

4.4 Scanning Electron Microscopy Sulfide Grain Size Distribution

All sulfide grains had sizes in the range of 2.4 to 1,200 micrometers. In general, the size distributions of each sulfide mineral were similar. The one exception was chalcopyrite which had fewer large sized particles, particularly in the 0.5-2.0 mm interval, than the rest of sulfides (table 4.6).

The 2.0-6.35 size fraction did not contain the largest sulfide minerals. Instead, the 0.5-2.0 mm size interval contained the largest sulfide minerals. This data is in contrast to visual inspection of the crushed sample where numerous sulfide grains were observed in sizes greater than 1,200 microns. It is likely that the limited sample size for the coarsest particle size fraction resulted in an inaccurate determination of the actual sulfide grain size distribution. Because of this apparent sample size limitation, the true sulfide grain size distribution for the 2.0-6.35 mm size interval may not have been determined. However, it is possible the larger sulfide grains may have been preferentially concentrated in the 0.5-2.0 mm size interval from the crushing process. Enrichment of the sulfide in the 0.5-2.0 mm fraction is supported by the greater sulfur concentration in that fraction (1.22 wt%) compared to the 2.0-6.35 mm fraction (1.05 wt%) which was less than the bulk sulfur concentration (1.24 wt%). It is not clear how much of an effect the sample size limitation for the coarsest fraction impacted the measured sulfide grain size distribution.

4.5 Sulfur Release Models

Two separate models, one empirical and the other theoretical, were developed to evaluate the rate at which sulfur was removed from the DCLP. The empirical model was constructed from leachate composition and volume data collected over a 38 year period. This model numerically describes the average annual amount of sulfur removed from a naturally weathering system and provides a basis for evaluating theoretical models.

The application of a theoretically based sulfide oxidation model has an extensive history of use in the fields of metallurgy (e.g., Levenspiel, 1972) and environmental science (Davis and Ritchie, 1986; Davis and Ritchie, 1987; Scharer et al., 1995; Wunderly et al., 1996; and Huminicki and Rimstidt, 2009). The most common theoretical models, employed to predict sulfide oxidation of natural systems, include the shrinking core and the shrinking particle models. In the environmental sciences, the shrinking core model is more commonly used because it accounts for the development of a reaction product coating on the surface of sulfide grains. For the shrinking core model, the rate of the oxidation reaction is limited by oxygen diffusion through the coating (e.g., an iron oxide coating or hydrated iron sulfate compounds, etc.). The theoretical model constructed in this report is based on the shrinking particle model as described by Rimstidt (2014). The shrinking particle model was selected because the low pH environment of the DCLP may not consistently result in substantial development of an iron oxide coating (e.g., ferrihydrite) on the sulfide surfaces. Previous SEM analyses and reflected light petrography studies have variably observed the presence of iron oxide coatings on sulfide mineral surfaces (see appendices in Lapakko et al., 2004). Geochemical modeling using the Geochemists Workbench software applying the Minteq thermodynamic database also indicates that ferrihydrite is variably saturated in the DCLP leachate (assuming one half the reporting limit for iron (0.005 mg/kg)). Regardless of whether or not iron oxide coatings are precipitating on the sulfide mineral surfaces, this study applies the shrinking particle model

as a simplified approach to assess how well a theoretical model, with thoroughly characterized rock material, compares to the empirically determined rate of sulfur removal.

4.5.1 Empirical Model

The empirical model incorporated the annual sulfate release rates reported in the Amax field study (Lapakko et al., 2004) and the more recent DCLP data set (Appendix 1). The empirical model was constructed in two parts due to the change in sulfate release rate over time. The first part is characterized by a linear regression model and the second as a power function regression model using Microsoft Excel software. The coefficients of determination (i.e., R^2 values) for the linear and power function regressions are 0.13 and 0.84, respectively. The p-value for the linear regression is 0.22, indicating a 78 percent confidence interval. For a single year, the average annual release rate was weighted by volume from each of the three Amax field study rock piles that the DCLP was constructed from. Annual release rates from years 1980, 1982, and 1985 were not included in the model due to either very low annual rainfall volume (1980) or an extremely elevated rainfall volume (1982 and 1985). The remaining 13 years of data were incorporated into a linear regression model to develop a mathematical expression for sulfur removal with time. Beginning in 1996, annual average sulfate release rates were calculated from the DCLP leachate composition and recorded leaching volume. Leachate composition and flow volume data is only available for 1996-1998, 2002, 2012, and 2015. In 2002, there was a substantially greater amount of rain fall during the late summer months (July through August) during which only one volume (80,345 L) and leachate sample was collected. Because such a large volume of leachate is represented by only one sulfate concentration measurement it is quite possible that the single value is not representative of the entire volume and only the last amount of leachate that passed through the system is represented. Therefore, this single sample event in 2002 was excluded to avoid misrepresentation of the data. The exclusion of data from 1980, 1982, 1985, and 2002 offers an empirical model that reflects more normal conditions and provides a consistent baseline model for comparison to the theoretical model which, likewise, does not include extreme events. The empirical model with regression line formulas is shown in figure 4.8. The data points used in the regression models are listed on table 4.8.

4.5.2 Theoretical Model

The theoretical model was constructed using physical and chemical data from a 14.7 kg composite rock sample collected from the DCLP that is described in section 3.3. The sole exception is that the rock pile volume weighted average sulfur content from the three original Amax field study rock piles was used (0.91 wt% sulfur) instead of the composite sample sulfur concentration (1.24 wt%). The volume weighted average incorporated 133 sulfur analyses from ‘blast rounds’ during the original excavation of the rock (Eger et al., 1980). This rock data was then incorporated into a shrinking particle model using a pyrrhotite oxidation rate determined from a laboratory batch flow reactor experiment. Pyrrhotite oxidation rates, like all mineral reactions, are strongly surface area dependent (eq. 2.1). Therefore, the total amount of sulfide surface area for the DCLP needed to be determined. For a mass of rock of different size particles both the sulfide grain size distribution and number of sulfide grains must be known to apply the shrinking particle model. For the theoretical model the sulfide grain size measurements were assumed to represent the diameter of a sphere. The number of sulfide spheres available for oxidation within a specific rock particle size interval (i) can be calculated using equation 4.1. The SA_{exp} and V_{sphere_i} parameters of eq. 4.1 were determined by SEM MLA methods described in section 4.1. The decision to only use the sulfide grains that are greater than 80% exposed was based on inspection of the MLA data on table 4.7. This table shows that there is a relatively small percentage of sulfide grains in the 30% to 80 % surface exposure ranges and only the two largest particle size intervals had a large amount of sulfides in the less than 30% exposed surface area range. Therefore, using only the fraction of grains that were greater than 80% surface area exposed incorporates the vast majority of the total sulfide surface area. Parameters and calculated values for eq. 4.1 are listed in table 4.9.

$$\# \text{ sulfide spheres}_i = M_i \times C_i \times \frac{P_{O_{mm}}}{S_{mm}} \div P_{O_{MW}} \times V_{m_{P_o}} \times SA_{exp} \div V_{sphere_i} \quad \text{eq. 4.1}$$

M_i = mass of particle size interval (kg)

C_i = rock sulfur concentration as $\text{g}_{\text{sulfur}} / 10 \text{ kg}_{\text{rock}}$

$\frac{P_{O_{mm}}}{S_{mm}}$ = pyrrhotite / sulfur molecular mass ratio

$P_{O_{MW}}$ = pyrrhotite molecular weight (82.3255 g/mole)

$V_{m_{P_o}}$ = pyrrhotite molecular volume ($1.82 \times 10^{-5} \text{ m}^3/\text{mole}$)

SA_{exp} = MLA determined sulfur wt% of >80 % surface area exposed

V_{sphere_i} = volume of average sulfide grain; P50 value from pyrrhotite MLA data

Once the number of sulfide spheres for each rock particle size fraction is determined, the shrinking particle model (in Rimstidt (2014); eq. 4.2) can be applied to calculate the amount of sulfur oxidized over time. The surface area normalized pyrrhotite oxidation rate of Bilenker et al. (2015; eq. 4.3) was used for the theoretical predictions assuming an atmosphere equilibrated fluid (oxygen saturated) with a pH of 4. This pyrrhotite oxidation rate was determined for sulfide oxidation in seawater, but is similar to other measured rates determined for specific pH values (fig. 4.9). The rate law of Bilenker et al. (2015) was selected because it was measured at a relatively constant temperature (about 22° Celsius) over a range of different fluid pH (2 to 6) and oxygen partial pressures (0.01 to 0.995 atm) values to fully characterize the pyrrhotite oxidation rate dependence on fluid pH and oxygen concentration (Romano, 2012). Other published pyrrhotite oxidation rates were measured for individual fluid pH values, used chelating agents, and/or did not specify the dissolved oxygen concentration (see references on fig. 4.9). The amount of sulfur oxidized at any given time can be calculated by the sphere volume calculated from the difference between D_t and D_o for all of the sulfide grains.

$$D_t = D_o - 2 \times k_{P_o} \times V_{m_{P_o}} \times t \quad \text{eq. 4.2}$$

$$k_{P_o} = -10^{-7.27} \times m_{O_2}^{0.30 \pm 0.07} \times m_{H^+}^{0.08 \pm 0.03} \quad \text{eq. 4.3}$$

D_t = grain diameter at time t

D_o =initial grain diameter

k_{P_o} = surface area normalized pyrrhotite oxidation rate ($\text{mol} \cdot \text{m}^{-2} \cdot \text{s}^{-1}$)

t = time (s)

m_{O_2} = molality aqueous oxygen

m_{H^+} = molality of hydronium ion

Two separate theoretical model calculations were performed. One used the DCLP volume weighted average of particle size interval masses from the FL1, FL5, and FL6 Amax field study rock piles and the other used the particle size interval masses for an individual sample collected from the FL4 rock pile in 1982, which had a greater amount of fine particles (see table 4.9). Figure 4.10 shows the theoretical model results as the cumulative amount of sulfur removed and the calculated values are listed in table 4.10. The early large slope is due to the greater specific surface area ($\text{m}^2 \cdot \text{kg}^{-1}$) of the fine fractions resulting in large amounts of sulfide being oxidized early in the system. Table 4.10 lists the percentages of sulfur removed at each one year interval relative to the total amount removed at year 38. Figure 4.11 shows the time at which sulfide grains from each of the rock particle size intervals have been entirely reacted. The early large sulfur removal slope, relative high percentages of sulfur removal, and theoretical indication of the fine sulfides being exhausted by year 15 clearly indicate that the initial removal of

sulfide is predominantly from the fine sulfide grains. After the fine sulfide grains have been exhausted, the rate at which sulfur is removed decreases (fig. 4.10).

4.5.3 Model Comparison

Figure 4.12 shows the sulfur removal trends for both the empirical and theoretical models. The theoretical models both under predict the removal of sulfur by year 12. The theoretical model incorporating a greater amount of fines over estimates the empirical model for the first 11 years whereas the other theoretical model very closely agrees with the empirical model for about the first five years. Figure 4.12 shows the relative percent difference of the theoretical models from the empirical model illustrating that both models are within a factor of 2 from the empirical model and that the greater fines example under predicts by about 30% after all of the finest grained sulfides have been removed.

5.0 DISCUSSION

Developing and comparing the two different model types has afforded the opportunity to elucidate the governing physical and hydrogeochemical parameters and determine how these parameters influence model results. Although the large copper and nickel concentrations of the rock modeled in this study may be considered ore by current standards, there are existing naturally weathering Duluth Complex waste rock piles that have similar copper, nickel and sulfur concentration (e.g., Dunka Mine and historic INCO shaft site). The results of this study are important for understanding weathering processes at those locations as well as assessing the general reactivity of potential future mine wastes with sulfur concentrations similar to the values modeled in this report. The following discussion describes the sensitivity of the empirical and theoretical models to some parameters, provides a general assessment of the modeling approach, and evaluates how the theoretical model could be improved.

5.1 Model Sensitivity

A number of studies have highlighted the importance of the smaller sized particles (namely sulfides) governing the leachate composition for rock weathering at the laboratory and field scales (Wenz et al., 2013; Lapakko et al., 2006; Stromberg and Banwart, 1999 and Doepker, 1994). Theoretically, the sulfide reaction rate is strongly dependent on the amount of surface area available for reaction (eq. 2.1). Applying basic geometry and a specified grain diameter and mineral density the total surface area of a mass can be calculated. An example of this calculation for 1 gram of pyrrhotite for different grain diameters is shown in table 4.11. This calculation shows the orders of magnitude increase in surface area for decreasing sulfide grain size. Relating the surface area data from table 4.11 to eq. 2.1 shows that the rate of pyrrhotite reaction increases by orders of magnitude from sub-millimeter to millimeter sized grains. This mathematical exercise clearly demonstrates that accurately constraining the amount and size distribution of the smallest sulfide grains is very important for modeling the release of sulfur from a mass of weathering rock.

To assess the sensitivity of the theoretical model used in this study the amount of the smaller sized rock particle intervals was increased using the greatest amount of fines measured from sieve analyses of the FL4 rock pile from the Amax field study (Lapakko et al., 2004). This resulted in substantially increasing the number of pyrrhotite spheres in the theoretical model (table 4.9). Comparison between the two different theoretical models showed that the model is very sensitive to small changes in the amount of small sized sulfide grains. Changing the mass fraction of the four smallest particle size intervals (by a combined amount of 0.037) increased the total amount of sulfur removed by about 50%. Therefore, a very accurate representation of the rock particle size distribution is necessary for applying the shrinking particle model.

For this data set, the MLA sulfide mineral exposure data was only valid for the fractions less than 2 mm because the required MLA sample size is too small to incorporate enough grains to accurately represent large size fraction intervals. To assess whether or not the 2.0-6.35 mm size fraction could substantially impact the overall model results, the theoretical model was extended to include the 2.0-6.35 mm particle size interval. This model extension assumed 50% of the sulfide grains were available and had an average diameter of 3.765 mm. For the extended model the total mass of sulfur removed at year 38 would only increase by 21 kg or about 4%. This demonstrated that even the 2.0-6.35 mm size fraction has little impact to the overall model results.

It is not clear how much of an impact rock particles greater than 6.35 mm would have on the overall model. Although the greater than 6.35 mm particles would have a relatively small sulfide surface area the 6.35-38.1 mm size fraction accounts for 37% of the total rock pile mass. Thus, despite the relatively small SSA of the larger particles the large percentage of mass for the 6.35-38.1 mm size range could influence the model results. The larger size fractions would not contribute much of the total sulfur removed early, but more likely would be responsible for the long term release of sulfate from the system. Including the greater than 2 mm sized particles into the theoretical model was not possible for this modeling exercise because of the limitation of the sulfide grain size measurements at about 1 mm. The sulfide grain size limitation is inherent to MLA analysis due to sample size requirements. A more complete sulfide grain size distribution would likely improve the theoretical model results.

The empirical model represents the average sulfate release rate from 1978 to 1993, excluding anomalous low and high annual precipitation years. Comparison among the actual annual sulfate release rates show up to a factor of three variation has occurred (table 4.8; years 1980 and 1982). Thus, in applying the type of modeling presented in this report for regulatory purposes, the effect of variable precipitation rates must be considered.

5.2 Model Interpretation

The difference in sulfur removal trends between the empirical and theoretical models for about the first 20 years indicates that the theoretical model is not accounting for some of the physical and/or hydrogeochemical mechanisms early in the weathering history (fig. 4.12). However, the general agreement in slope between the empirical and theoretical models after about 20 years indicates that the theoretical model may be accurately characterizing the various hydrogeochemical mechanisms. Some of the more obvious factors responsible for the disagreement include the 1) accuracy of the exposed sulfide surface area calculations, 2) efficiency of sulfide oxidation products removal, and 3) representativeness of the shrinking particle model.

The accuracy of the exposed sulfide surface area calculations is dependent on the mass of the particle size intervals and representativeness of the MLA determined sulfide surface area measurements. Figure 4.11 shows that at about year 15 the smallest sized sulfide particles (less than 0.053 micron particle fraction) are entirely reacted. Based on comparison to the empirical model, this may indicate that the amount of smaller sized particles used in the theoretical model is wrong because a greater amount of fine material would have raised the magnitude of the sulfide removal trend up to the level of the empirical model. Alternatively, not accounting for the partially exposed sulfide grains may have resulted in a greater amount of sulfide removal than was accounted for in the theoretical model.

The difference in sulfur removal trends may also be due to differences in the efficiency of sulfide oxidation product removal (e.g., sulfate). The theoretical model calculation sums the mass of reacted material at each time step, whereas in a natural setting the sulfate that is transported in the leachate may not represent the entire mass of reacted material with time because it could be stored in the waste rock pile. In effect, the overall removal of sulfur via sulfide oxidation is slowed because infiltrating water does

not collect all of the reactant products. Considering the likely possibility of sulfur storage and limited water contact, the theoretical model which incorporated a greater amount of fines is more likely because the overall greater mass and rate of sulfur removal should exceed that of the empirical model that inherently contains reaction product release limitations.

The application of the shrinking particle model is a reasonable first approximation. However, it is likely that some reaction products have precipitated on some of the mineral surfaces. The extent to which the coating may limit the rate of sulfide oxidation depends on the specific type (composition and morphology) of coating that develops. Numerous investigators have reported accumulation of sulfide compounds on the pyrrhotite mineral surface during oxidation (e.g., Buckley and Woods, 1985 and Steger, 1982). However, it is unclear if these reaction products are precipitates or if they represent specific half reactions for the overall oxidation reaction (i.e., rxn. 2.1). Furthermore, applying the shrinking core model requires knowledge of the diffusion rate of oxygen through the developed coating. Although some studies have calculated the diffusion rate for coatings on pyrite (e.g., Huminicki and Rimstidt, 2009 and Jerz and Rimstidt, 2004), there are no available oxygen diffusion rates for reaction product coatings on pyrrhotite.

Ultimately, the differences between the empirical and theoretical models are most likely a combination of factors described in the preceding paragraphs. Determining the proportion of which is responsible for the model differences is not possible without a more robust characterization of the system. For example, using the shrinking particle model instead of the shrinking core model may have resulted in a greater amount of sulfur removal for the theoretical model whereas the actual greater release in the empirical model was due to oxidation of the partially exposed sulfide grains that were not accounted for in the theoretical model. Furthermore, storage of sulfate in the rock pile may also account for a lower measured sulfur removal compared to the theoretical model which accounted for the total mass of reacted sulfur.

After about year 20, all three of the models generally exhibit the same sulfur removal trend (fig. 4.12). This implies that the remaining sulfide amount and size distributions are similar among the models. Thus, the overall lower magnitude of sulfur removed in the theoretical models is likely due to either inaccurate measurements of rock particle and sulfide mineral grain abundance and size distribution, or some other unidentified parameter that accelerated the rate of sulfur removal in the field.

5.3 Model Improvement

The close agreement between the empirical and theoretical model results demonstrates that relatively accurate theoretical prediction models can be developed with minimal data input. Despite the simplifying assumptions (e.g., constant fluid pH, all sulfur in the form of pyrrhotite, etc.) incorporated into the theoretical model, there was less than a factor of two difference between the empirical and theoretical models for the 38 year record. Although a factor of two difference is generally not considered very accurate, in terms of evaluating mine waste management options that level of accuracy can guide mine waste management decisions. Decreasing the variability and uncertainty of the input parameters and incorporation of additional hydrogeochemical parameters will likely improve the predictive capability of the theoretical approach.

This modeling exercise has indicated that the shrinking particle model can be a feasible approach for predicting sulfur release from waste rock with a small leachate pH if the physical parameters (e.g., particle size distribution, sulfide grain size, and amount of sulfide grain surface exposure) of the system are accurately characterized. For circumneutral pH environments the shrinking particle model is less likely to be applicable because ferrihydrite is not soluble and iron-oxide rims would most likely develop on the sulfide surfaces. Accurately quantifying the amount of the small sized rock particles is difficult due to the small sample size typically employed for sieve analysis. This theoretical model incorporated three

particle size interval wt% measurements from the Amax field study. Increasing the number of weighted particle size interval measurements would likely improve the accuracy of the model. Another important parameter is the amount of sulfide surface area exposed. In this exercise only the material less than 2 mm was used to calculate the total mass of sulfur removed. The 2 mm cut off was based on the MLA sulfide exposure values of the less than 6.35 mm material. However, both stereo microscope inspection of the greater than 2 mm sized material used for MLA and field observation of the DCLP qualitatively revealed that millimeter sized sulfide grains are more common than that determined by the MLA analysis. Further refinement of this modeling approach should include accounting for the additional sulfide surface area on the greater than 2 mm sized material. Of particular importance is accurately accounting for all of the sulfide that is readily available for oxidation during the first few years of weathering.

The theoretical model used in this report applied a stepped size interval approach to apply the shrinking particle model in which the average (P50) sulfide size was applied for each size interval. Further refinement could be incorporated by applying the actual MLA determined sulfide grain size distribution for each of the particle size intervals. This was not possible with the existing data because the wt% of exposed sulfide surface area was determined for each of the rock particle size intervals and not the sulfide grain size distribution.

Petrographic analysis of the fine materials would provide visual evidence of whether or not reaction products are coating the different sulfide minerals. In addition, petrography would also provide information on the competency of the surface coatings. Assessing the competency of the coatings could indicate if there is a diffusion limitation or if there are fractures in the coating and parting along the coating and sulfide interface that may be more accurately represented by a shrinking particle model.

Determining the relationship among infiltration volume, leachate concentration, and time between precipitation events could inform the type and value of hydrologic parameters that could be incorporated into the theoretical model. Evaluating this relationship could be accomplished by more intensive monitoring of the leachate volume and greater frequency of leachate chemical analysis.

6.0 ACKNOWLEDGEMENTS

Over the years, MN DNR Hibbing staff (Pat Gieselman, Dave Antonson, Doug Rosnau, and Steve Koski) have maintained the operation of the DCLP and treatment center and collected the leachate samples for chemical analysis. Funding for this report and data collected in 2014 and 2015 was provided by the state of Minnesota Cooperative Environmental Research (CER) program with contributions from PolyMet Mining Inc., Mining Minnesota, and The North Central Mineral Venture. Previous funding was provided by the Minnesota State General Fund.

7.0 REFERENCES

- Bilenker L.D., Romano G.Y., and McKibben M.A. 2015. Kinetics of sulfide mineral oxidation in seawater: Implications for acid generation during *in situ* mining of seafloor vents. Goldschmidt Abstracts, no. 299.
- Buckley, A.N., and Woods, R. 1985. X-ray photoelectron spectroscopy of oxidized pyrrhotite surfaces: I Exposure to air. *Applications of Surface Science*. v.22, p. 280-287.
- Davis, G.B. Ritchie, A. I. M. 1986. A model of oxidation in pyritic mine wastes: part 1: equations and approximate solution. *Applied Mathematical Modelling*, v. 10, p. 314-322.
- Davis, G.B., Ritchie, A. I. M. 1987. A model of oxidation in pyritic mine wastes: part 3: import of particle size distribution. *Applied Mathematical Modelling*, v. 11, p. 417-422.
- Doepeker, R.D. 1994. Laboratory determination of parameters influencing metal dissolution from sulfidic waste. *International Journal of Surface Mining, Mining, Reclamation and Environment*, v. 8, p. 55-63.
- Eger, P., Johnson, B., and Hohenstein, G. 1979. 1978 DNR/AMAX field leaching and reclamation program. Progress report on the leaching study, Minnesota Department of Natural Resources. 160 p.
- Eger, P., Lapakko, K., Weir, A. 1980. Heavy metals study: 1979 progress report on the field leaching and reclamation program and the removal of metals from stockpile runoff by peat and tailings, Minnesota Department of Natural Resources. 95 p. plus appendices.
- Eger, P., and Lapakko, K.A. 1985. Heavy metals study: Progress report on the field leaching and reclamation program: 1977-1983. Minnesota Department of Natural Resources. 53 p. plus appendices.
- Fala, O., Molson, J., Aubertin, M., and Bussiere, B. 2005. Numerical modelling of flow and capillary barrier effects in unsaturated waste rock piles. *Mine Water and the Environment*, v. 24, p. 172-185.
- Holmes, P.R., and Crundwell, F.R. 2000. The kinetics of the oxidation of pyrite by ferric ions and dissolved oxygen: An electrochemical study. *Geochimica et Cosmochimica Acta*, v. 64, p. 263-274.
- Huminicki, D.M.C., and Rimstidt, J.D. 2009. Iron oxyhydroxide coating of pyrite for acid mine drainage control. *Applied Geochemistry*, v. 24, p. 1626-1634.
- Janzen, M.P., Nicholson, R.V., and Scharer, J.M. 2000. Pyrrhotite reaction kinetics: Reaction rates for oxidation by oxygen, ferric iron, and for nonoxidative dissolution. *Geochimica et Cosmochimica Acta*, v. 64, p. 1511-1522.
- Jerz, J.K., and Rimstidt, J.D. 2004. Pyrite oxidation in moist air. *Geochimica et Cosmochimica Acta*, v. 68, p. 701-714.
- Kellogg, C., Lapakko, K.A., Olson, M.C., Jenzen, E., Antonson, D.A. 2014. Laboratory dissolution of blast hole samples of Duluth Complex rock from the South Kawishiwi Intrusion: Twenty-four year laboratory experiment. Minnesota Department of Natural Resources. 314 p. plus appendices.

- Kimball, B.E., Rimstidt, J.D., and Brantley, S.L. 2010. Chalcopyrite dissolution rate laws. *Applied Geochemistry*, v. 25, p. 972-983.
- Kwong, E.C.M. 1995. Abiotic and biotic pyrrhotite dissolution. M.S. thesis. University of Waterloo, Waterloo, Ontario.
- Lapakko, K.A. 1993. Field dissolution of test piles of Duluth Complex rock. Minnesota Department of Natural Resources. 41 p. plus appendices.
- Lapakko, K.A., Olson, M.C., and Antonson, D.A. 2013. Dissolution of Duluth Complex rock from the Babbitt and Dunka Road Prospects: Eight-year laboratory experiment. Minnesota Department of Natural Resources. 88 p. plus appendices.
- Lapakko, K.A., Antonson, D.A., Engstrom, J.N. 2004. Analytical screening of abandoned waste rock piles. Minnesota Department of Natural Resources. 91 p. plus appendices.
- Lapakko, K. A., Engstrom, J. N., Antonson, D. A. 2006. Effects of particle size on drainage quality from three lithologies. In proceedings, 7th International Conference on Acid Mine Drainage, St. Louis, Missouri, 33 p.
- Levenspiel, O. 1972. *Chemical Reaction Engineering*, 1st edition, Wiley, New York, 578 p.
- McKibben, M.A., and Barnes, H.L. 1986. Oxidation of pyrite in low temperature acidic solutions: Rate laws and surface textures. *Geochimica et Cosmochimica Acta*, v. 50, p. 1509-1520.
- Miller, J.D., Jr., Green, J.C., Severson, M.J., Chandler, V.W., Hauck, S.A., Peterson, D.M., and Wahl, T.E. 2002. Geology and mineral potential of the Duluth Complex and related rocks of northeastern Minnesota: Minnesota Geological Survey Report of Investigations 58, 207 p.
- Nicholson, R.V., and Scharer, J.M. 1994. Laboratory studies of pyrrhotite oxidation kinetics. *In: American Chemical Society Symposium Series, Chapter 2: Environmental Geochemistry of Sulfide Oxidation*. P. 14-30.
- Palandri, J.L., and Kharaka, Y.K. 2004. A compilation of rate parameters of water-mineral interaction kinetics for application to geochemical modeling. U.S. Geological Survey Open File Report 2004-1068. U.S. Geological Survey in cooperation with the National Energy Technology Laboratory - United States Department of Energy, 70 p.
- Rimstidt, J.D., 2014. *Geochemical rate models: an introduction to geochemical kinetics*. 1st edition, Cambridge University Press, New York. 232 p.
- Romano, G.Y. 2012. Kinetics of pyrrhotite oxidation in seawater: Implications for mining seafloor hot springs. Master of science thesis, University of California Riverside. 79 p.
- Scharer, J.M., Kwong, E.C.M., Nicholson, R.V., Pettit, C.M., and Chambers, D.W. 1995. Factors affecting ARD production: Kinetics of sulphide oxidation. *In: Sudbury '95: Mining and the environment: Sudbury, Canada, May 28 to June 1, 1995: Conference proceedings*. P. 451-459.
- Steger, H.F. 1982. Oxidation of sulfide minerals: VII. Effect of temperature and relative humidity on the oxidation of pyrrhotite. *Chemical Geology*. V. 35, p. 281-295.

- Stromberg, B., and Banwart, S.A. 1999. Experimental study of acidity-consuming processes in mining waste rock: some influences of mineralogy and particle size. *Applied Geochemistry*, v. 14, p. 1-16.
- Wenz, Z., Lapakko, K. A., Antonson, D. A. 2013. Rock composition, leachate quality and solute release as a function of particle size for three waste rock types: An 18-year laboratory experiment. Minnesota Department of Natural Resources. 106 p. plus appendices.
- Williamson, M.A., Rimstidt, J.D. 1994. The kinetics and electrochemical rate-determining step of aqueous pyrite oxidation. *Geochimica et Cosmochimica Acta*, v. 58, p. 5443-5454.
- Wunderly, M.D., Blowes, D.W., Frind, E.O. and Ptacek, C.J., 1996. Sulfide mineral oxidation and subsequent reactive transport of oxidation products in mine tailings impoundments: A numerical model. *Water Resources Research*, v. 32 p. 3173-3187.

Table 4.1 Bulk and particle size interval XRD and MLA mineralogy. Values are in as weight percent.

Mineral (Wt%)	XRD	Mineral Liberation Analysis					
	Bulk	Bulk	2.0-6.35	0.5-2.0	0.149-0.5	0.053-0.149	< 0.053
Amorphous	12.9	--	--	--	--	--	--
Amphibole	--	14.24	10.64	9.86	10.15	13.12	16.97
Apatite Cl	--	0.25	0.51	0.32	0.53	0.93	1.1
Augite (Cpx)	7.5	8.46	6.18	15.18	8.87	7.05	7.42
Baddeleyite	--	--	--	--	--	--	0.04
Biotite	2.7	3.28	1.83	1.54	2.57	1.96	1.04
Chlorite	--	1.24	0.53	1.6	1.04	1.11	1.36
Cordierite	2.2	--	--	--	--	--	--
Enstatite (Opx)	6.2	20.52	15.44	12.08	16.25	15.72	13.68
Epidote	--	0.43	0.14	0.38	0.32	0.19	0.4
Fe Silicate clay	--	--	--	0.01	0.05	0.21	0.2
K-feldspar	--	0.28	1.65	0.48	0.47	0.43	0.46
Muscovite	--	0.09	0.07	0.05	0.08	0.05	0.07
Olivine (Forsterite)	8.9	--	--	--	--	--	--
Plagioclase	55.5	40.79	54.18	44.36	38.2	37.42	32.81
Quartz	--	--	--	0.07	0.21	0.22	0.38
Smectite	--	0.04	0.01	0.06	0.04	0.04	0.06
Talc	--	0.01	--	--	0.08	0.05	0.02
Zircon	--	0.01	0.03	--	--	--	0.03
Fe (O,OH)	--	0.05	--	0.07	0.66	0.63	1.49
Ilmenite	2.6	7.25	7.59	6.54	12.33	9.3	8.3
Calcite	--	0.02	--	0.01	0.04	0.05	0.06
Siderite	--	0.06	0.02	0.05	0.28	0.34	0.62
Bornite	--	0.01	0.03	--	--	0.02	0.04
Chalcopyrite	0.5	0.52	0.39	1.66	0.77	1.06	2.17
Cubanite	1	1.05	0.42	3.57	3.36	5.8	6.81
Pentlandite	--	0.17	0.02	1.62	1.36	1.12	1.61
Pyrrhotite	--	0.74	0.06	0.13	1.88	2.5	1.7
FeCuNi Sulphate	--	0.06	0.01	0.07	0.09	0.18	0.62
Others	--	0.44	0.23	0.29	0.39	0.51	0.54
Total	100	100	100	100	100	100	100

Table 4.2 Bulk sample major oxide concentrations.

Size Interval (mm)	SiO ₂ wt%	Al ₂ O ₃ wt%	Fe ₂ O ₃ wt%	MnO wt%	MgO wt%	CaO wt%	Na ₂ O wt%	K ₂ O wt%	TiO ₂ wt%	P ₂ O ₅ wt%	LOI	Total
2.0-6.35 mm	44.66	15.94	16.97	0.169	6.83	8.76	2.26	0.51	2.268	0.25	-0.27	98.35
0.5-2.0 mm	45.06	15.62	17.17	0.171	6.75	8.8	2.29	0.5	2.317	0.15	-0.24	98.57
0.149-0.5	43.85	16.15	17.33	0.167	6.2	8.46	2.36	0.56	2.82	0.2	-0.19	97.89
0.053-0.149	43.22	15.38	17.99	0.178	6.33	8.18	2.26	0.53	2.886	0.37	0.19	97.51
< 0.053	42.83	15.68	18.03	0.185	6.35	8.22	2.17	0.41	3.086	0.5	0.86	98.31
Bulk	45.01	16.02	17.25	0.171	6.82	8.66	2.24	0.51	2.37	0.19	-0.18	99.06

Size interval (mm)	SiO ₂ wt%*	Al ₂ O ₃ wt%*	Fe ₂ O ₃ wt%*	MnO wt%*	MgO wt%*	CaO wt%*	Na ₂ O wt%*	K ₂ O wt%*	TiO ₂ wt%*	P ₂ O ₅ wt%*
2.0-6.35 mm	44.93	16.72	17.01	0.17	7.06	8.95	--	0.48	2.30	0.18
0.5-2.0 mm	44.50	16.67	17.01	0.17	6.92	8.88	--	0.48	2.32	0.15
0.149-0.5 mm	43.64	16.72	17.59	0.18	6.38	8.72	--	0.48	2.84	0.20
0.053-0.149 mm	43.21	16.17	18.73	0.18	6.58	8.63	--	0.48	2.94	0.36
< 0.053 mm	42.14	15.44	20.16	0.20	6.67	8.55	--	0.36	3.00	0.50
Bulk	45.35	16.63	17.16	0.18	7.08	8.97	--	0.60	2.42	0.19

* Indicates oxide values calculated from the elemental wt% values determined from sodium peroxide fusion and ICP-MS analysis.

Table 4.3 Bulk sample and particle size interval total sulfur, carbon, chloride, fluoride, and bromide concentrations.

Size Interval (mm)	C _T wt% ¹	S _T wt% ¹	S _T wt%*	Cl wt%	F wt%	Br (ppm)	C _T wt% ²	S _T wt% ²	C _T wt% ³	S _T wt% ³
2.0-6.35	0.03	1.07	1.04	0.04	< 0.01	< 0.5	0.04	1.02	0.04	1.05
0.5-2.0	0.03	1.28	1.23	0.06	< 0.01	< 0.5	0.05	1.15	0.04	1.22
0.149-0.5	0.04	1.68	1.63	0.03	< 0.01	< 0.5	0.04	1.83	0.04	1.76
0.053-0.149	0.07	1.92	1.89	0.08	< 0.01	< 0.5	0.06	1.92	0.06	1.92
< 0.053	0.12	2.31	2.39	0.04	< 0.01	< 0.5	0.08	2.33	0.10	2.32
Bulk	0.03	1.22	1.22	0.04	< 0.01	< 0.5	0.03	1.25	0.03	1.24

* Values determined from sodium peroxide fusion and ICP-MS analysis.

¹ Analyses performed by Actlabs.

² Analyses performed by Lerch Brothers Inc. Hibbing, MN

³ Average values of the sulfur and carbon combustion analyses.

Table 4.4 Bulk and particle size interval trace metal and nonmetal analyses. Concentrations are in parts per million.

Size Interval (mm)	Cu	Ni	V	V*	Sr	Sr*	Ba	Ba*	Zn	Cr	Co	Zr*	B	Li	Se	Ga	Pb	Rb
2.0-6.35	6320	1100	349	254	295	264	220	199	170	160	106	116	60	12	19.9	22.6	14	13.5
0.5-2.0	6780	1390	325	247	291	265	298	279	220	190	121	95	80	12	11.9	21.8	18.7	13.4
0.149-0.5	8100	2110	356	259	300	266	208	200	200	170	154	131	100	12	27.3	23.3	24.8	15.3
0.053-0.149	9610	2220	350	273	286	255	568	493	410	170	159	182	90	19	18	21.6	205	13.7
< 0.053	>10000	2950	365	271	277	254	163	153	230	180	199	224	110	11	17	21.2	33.6	9.9
Bulk	6630	1420	346	258	283	264	187	183	170	150	122	107	90	30	25.6	21.6	16.1	14
Size Interval (mm)	Nb	Ge	Mo	Cs	Sn	Ta	Hf	Te	As	Bi	Cd	Sb	Be	Be*	W	In	Tl	
2.0-6.35	11.6	5.4	5	0.9	< 0.5	0.7	< 10	< 6	7	< 2	< 2	< 2	< 4	1	< 0.7	< 0.2	< 0.1	
0.5-2.0	9.9	4.2	1	0.9	1.2	0.5	< 10	< 6	82	< 2	< 2	< 2	< 4	< 1	< 0.7	< 0.2	< 0.1	
0.149-0.5	15.5	4.2	3	0.8	5.1	1.2	< 10	< 6	< 5	< 2	< 2	< 2	< 4	< 1	< 0.7	< 0.2	< 0.1	
0.053-0.149	12.7	5.5	2	1	19.2	0.6	< 10	< 6	16	< 2	< 2	< 2	< 4	< 1	< 0.7	< 0.2	< 0.1	
< 0.053	13.9	5.2	3	0.7	91.8	0.7	< 10	< 6	11	< 2	< 2	< 2	< 4	< 1	1	< 0.2	< 0.1	
Bulk	10.5	5.2	3	1	0.5	0.3	< 10	< 6	< 5	< 2	< 2	< 2	< 4	< 1	< 0.7	< 0.2	< 0.1	
Size Interval (mm)	Sc*	Y	Y*	La	Ce	Pr	Nd	Sm	Eu	Gd	Tb	Dy	Ho	Er	Tm	Yb	Th	U
2.0-6.35	20	20.8	16	15.1	38.8	4.7	19.5	4.5	1.8	4.6	0.6	4	0.8	2.3	0.3	2	2.9	0.7
0.5-2.0	21	18.5	15	11.9	25.6	3.3	14.7	3.6	1.7	4	0.6	3.6	0.7	2	0.3	2.1	1.3	0.2
0.149-0.5	20	20.3	17	127	344	24.7	111	9.8	1.8	7	0.7	4	0.8	2.1	0.3	1.9	216	4.6
0.053-0.149	19	26.2	21	18.4	42.4	5.6	24.4	5.7	1.8	5.9	0.9	5	1	2.7	0.4	2.4	2.2	0.6
< 0.053	19	32.6	22	22.1	52	6.8	31.7	7.2	1.7	7.7	1.1	6.1	1.1	3.1	0.4	2.5	3.2	1.1
Bulk	21	20.2	16	14.6	33.1	4.1	18.8	4.3	1.8	4.4	0.6	3.9	0.8	2.2	0.3	2	2.2	0.4

* Lithium metaborate-tetraborate fusion and ICP-MS analysis.

Table 4.5 Mass weighted particle size sieve analysis.

Size Interval (mm)	Lerch Bros.				Actlabs		Average
	mass (g) dry	mass (g) wet	wt% dry	wt% wet	mass (g) dry	wt% dry	wt% dry
2.0-6.35	120	120.4	60	60.2	95	58.64	59.32
0.5-2.0	49	49.6	24.5	24.8	39	24.07	24.29
0.149-0.5	17.7	17.3	8.85	8.65	17	10.49	9.67
0.053-0.149	8.8	8	4.4	4	8	4.94	4.67
< 0.053	4.5	4.7	2.25	2.35	3	1.85	2.05
total=	200	200	100	100	162	100	100

Table 4.6 MLA determined sulfide grain size distribution. Values are in wt% passing.

		Cubanite				
		Particle Size Interval (mm)				
Grain Size (µm)		2.0-6.35	0.5-2.0	0.149-0.5	0.053-0.149	< 0.053
1.75		0	0	0	0	0
2.4		0	0	0	0	0.01
3.4		0	0	0.01	0	0.02
4.8		0.25	0.04	0.07	0.05	0.1
6.8		0.87	0.12	0.16	0.15	0.33
9.6		2.25	0.28	0.36	0.33	0.8
13.5		4.23	0.55	0.76	0.74	2
19		6.96	0.93	1.35	1.38	5.76
27		9.72	1.41	2.41	3.05	20.69
38		15.48	2.3	3.62	6.68	50.29
53		21.91	3.15	5.24	15.63	87.55
75		31.86	4.82	7.81	35.33	100
106		43.37	6.54	11.55	60.83	0
150		57.97	10.12	21.43	89.41	0
212		88.41	15.36	47.12	100	0
300		100	20.65	69.24	0	0
425		0	32.27	93.57	0	0
600		0	44.83	100	0	0
850		0	65.1	0	0	0
1200		0	100	0	0	0

		Pentlandite				
		Particle Size Interval (mm)				
Grain Size (µm)		2.0-6.35	0.5-2.0	0.149-0.5	0.053-0.149	< 0.053
1.75		0	0	0	0	0
2.4		0	0	0	0	0.01
3.4		0	0	0	0	0.03
4.8		0.63	0.22	0.11	0.05	0.08
6.8		1.57	0.59	0.31	0.2	0.29
9.6		3.12	1.17	0.58	0.35	0.71
13.5		9.5	1.91	1	0.69	2.06
19		14.75	2.93	1.44	1.06	5.78
27		21.12	4.11	1.89	2.66	23.09
38		47.67	4.81	2.35	5.72	60.79
53		67.53	6.21	2.74	14.17	91.93
75		100	6.8	4.25	29.6	100
106		0	9.05	7.78	53.72	0
150		0	12.66	13.42	80.81	0
212		0	12.66	28.78	100	0
300		0	12.66	51.83	0	0
425		0	12.66	70.48	0	0
600		0	12.66	100	0	0
850		0	12.66	0	0	0
1200		0	100	0	0	0

		Pyrrhotite				
		Particle Size Interval (mm)				
Grain Size (µm)		2.0-6.35	0.5-2.0	0.149-0.5	0.053-0.149	< 0.053
1.75		0	0	0	0	0
2.4		0	0	0	0	0.01
3.4		0	0	0	0	0.03
4.8		0.4	0.04	0.01	0.03	0.09
6.8		1.32	0.16	0.03	0.07	0.35
9.6		3.9	0.3	0.11	0.16	0.96
13.5		9.12	0.68	0.24	0.36	2
19		15.74	1.29	0.41	0.75	5.55
27		25.52	2.26	0.67	2.07	19.34
38		37.83	3.32	0.86	4.38	51.38
53		47.83	5.74	1.39	11.6	86.61
75		62.44	7.31	2.51	28.61	100
106		100	10.53	4.47	56.16	0
150		0	12.58	10.37	83.46	0
212		0	20.09	19.66	100	0
300		0	20.09	51.82	0	0
425		0	33.44	79.41	0	0
600		0	33.44	100	0	0
850		0	100	0	0	0

		Chalcopyrite				
		Particle Size Interval (mm)				
Grain Size (µm)		2.0-6.35	0.5-2.0	0.149-0.5	0.053-0.149	< 0.053
1.75		0	0	0	0	0
2.4		0	0	0.01	0.01	0.02
3.4		0	0	0.02	0.04	0.04
4.8		0.3	0.21	0.14	0.24	0.19
6.8		1.92	1.11	0.52	0.75	0.54
9.6		5.32	2.77	1.27	1.77	1.46
13.5		10.88	6.25	2.72	3.48	2.95
19		18.38	10.04	4.59	6.06	7.07
27		26.68	16.41	7.26	10.03	23.76
38		38.89	23.1	9.71	14.36	55.1
53		45.88	30.94	12.58	27.25	86.21
75		61.88	44.28	16.69	51.28	100
106		71.5	49.89	23.22	73.14	0
150		82.08	61.33	35.04	96.74	0
212		100	69.07	48.95	100	0
300		0	83.02	78.75	0	0
425		0	100	100	0	0
600		0	0	0	0	0
850		0	0	0	0	0

Table 4.7 MLA determined sulfide surface area exposed in wt%.

Pyrrhotite												
Size Interval (mm)	0%	0%-10%	10%-20%	20%-30%	30%-40%	40%-50%	50%-60%	60%-70%	70%-80%	80%-90%	90%-100%	100%
2.0-6.35	4.7	92.97	0	0	0	0	0	0	0	0	0	2.33
0.5-2.0	2.29	11.05	6.63	13.45	0	0	0	0	0	66.57	0	0
0.149-0.5	0.22	1.06	0.72	0.37	3.09	0.72	2.06	9.28	0.2	1.74	41.51	39.01
0.053-0.149	0.11	0.47	0.19	0.8	0.96	1.6	2.02	2.75	3.1	3.36	11.41	73.22
< 0.053	0	0.28	0.42	1.21	1.14	1.53	4.92	4.44	3	5.47	4.02	73.57
Cubanite												
Size Interval (mm)	0%	0%-10%	10%-20%	20%-30%	30%-40%	40%-50%	50%-60%	60%-70%	70%-80%	80%-90%	90%-100%	100%
2.0-6.35	6.02	93.59	0.4	0	0	0	0	0	0	0	0	0
0.5-2.0	0.69	12.26	9.25	5.44	0.79	13.59	2.65	0.1	0	9.7	19.61	25.92
0.149-0.5	0.69	3.12	1.81	2.08	4.05	1.97	3.13	1.97	1.5	6.35	19.7	53.63
0.053-0.149	0.12	0.75	0.47	0.98	1.08	0.95	1.13	1.59	0.73	4.28	5.71	82.21
< 0.053	0.01	0.32	0.61	0.93	1.29	2.36	2.44	3.71	2.97	4.9	5.13	75.34
Chalcopyrite												
Size Interval (mm)	0%	0%-10%	10%-20%	20%-30%	30%-40%	40%-50%	50%-60%	60%-70%	70%-80%	80%-90%	90%-100%	100%
2.0-6.35	16.57	82.94	0	0	0	0	0	0	0	0	0	0.5
0.5-2.0	6.46	59.13	8.34	25.57	0	0	0	0	0	0	0	0.5
0.149-0.5	3.03	11.77	3.41	3.01	1.33	0	0.68	1.52	8.75	6.99	26.97	32.55
0.053-0.149	1.26	5.32	2.7	2.07	3.46	1.6	2.6	1.21	0.51	7.42	2.01	69.86
< 0.053	0.26	0.72	1.63	2.67	1.66	1.87	4.26	3.33	5.9	6.24	2.78	68.66
Pentlandite												
Size Interval (mm)	0%	0%-10%	10%-20%	20%-30%	30%-40%	40%-50%	50%-60%	60%-70%	70%-80%	80%-90%	90%-100%	100%
2.0-6.35	43.28	56.72	0	0	0	0	0	0	0	0	0	0
0.5-2.0	3.25	9.37	0	0	0	0	0	0	0	0	87.39	0
0.149-0.5	0.5	1.53	0.06	3.05	0.44	0.03	0.83	0	2.66	17.63	53.53	19.74
0.053-0.149	0.16	0.7	0.29	0.66	0.2	0.92	0.58	0.99	2.95	13.75	19.49	59.3
< 0.053	0.06	0.37	1.03	1.12	1.21	2.76	1.42	2.22	4.76	6.58	4.79	73.67

Table 4.8 Measured sulfate release rates from the Amax field study composite and the DCLP.

Calendar Year	Model Year	Annual sulfate release rate (mmol·kg ⁻¹ ·wk ⁻¹)
1978	1	3.33E-02
1979	2	4.74E-02
1980	3	2.75E-02
1981	4	4.41E-02
1982	5	8.39E-02
1983	6	4.77E-02
1984	7	3.75E-02
1985	8	8.14E-02
1986	9	4.49E-02
1987	10	5.28E-02
1988	11	5.27E-02
1989	12	6.00E-02
1990	13	3.85E-02
1991	14	5.67E-02
1992	15	4.02E-02
1993	16	4.68E-02
1996	19	2.62E-02
1997	20	1.41E-02
1998	21	2.14E-02
2002	25	2.28E-02
2012	35	4.72E-03
2015	38	8.61E-03

Table 4.9 Theoretical model sulfide sphere calculations and parameter values for each of five particle size intervals.

Particle Size Interval (mm)	Average sulfide volume (m ³)	DCLP Mass (kg)	DCLP size interval mass fraction	DCLP greater fines mass fraction	sulfur (g/kg _{rock})	Pyrrhotite / Sulfur molecular mass ratio	Pyrrhotite (m ³ /mole)	>80% sulfide surface area available	# Pyrrhotite spheres (from volume weighted size interval mass fraction)	# Pyrrhotite spheres (from greater fines mass fraction)
2.0-6.35	9.33E-14	812,146	0.063	0.077	10.7	2.5675	1.82E-05	0	0	0
0.5-2.0	1.52E-10	812,146	0.031	0.05	12.8	2.5675	1.82E-05	0.50	601,492,692	970,149,503
0.149-0.5	1.34E-11	812,146	0.022	0.031	16.8	2.5675	1.82E-05	0.81	10,265,560,336	14,465,107,747
0.053-0.149	5.09E-13	812,146	0.011	0.015	19.2	2.5675	1.82E-05	0.90	172,101,963,643	234,684,495,877
<0.053	2.77E-14	812,146	0.009	0.014	23.1	2.5675	1.82E-05	0.84	2,910,859,056,830	4,528,002,977,291

Table 4.10 Theoretical calculation of cumulative mass of sulfur removed.

Model year	Mass of sulfur removed (kg)		Percentage of sulfur removed	
	Volume weighted composite	Greater fines	Volume weighted composite	Greater fines
1	46	68	8.8%	8.9%
2	87	130	7.8%	8.1%
3	125	186	7.3%	7.3%
4	159	236	6.5%	6.6%
5	190	281	5.9%	5.9%
6	217	322	5.2%	5.4%
7	242	357	4.8%	4.6%
8	263	389	4.0%	4.2%
9	283	418	3.8%	3.8%
10	301	443	3.4%	3.3%
11	316	466	2.9%	3.0%
12	330	486	2.7%	2.6%
13	343	504	2.5%	2.4%
14	355	521	2.3%	2.2%
15	366	537	2.1%	2.1%
16	377	552	2.1%	2.0%
17	387	566	1.9%	1.8%
18	397	580	1.9%	1.8%
19	406	593	1.7%	1.7%
20	415	606	1.7%	1.7%
21	423	618	1.5%	1.6%
22	432	630	1.7%	1.6%
23	439	641	1.3%	1.4%
24	447	652	1.5%	1.4%
25	454	662	1.3%	1.3%
26	461	672	1.3%	1.3%
27	467	681	1.1%	1.2%
28	473	690	1.1%	1.2%
29	479	699	1.1%	1.2%
30	485	707	1.1%	1.0%
31	490	715	1.0%	1.0%
32	496	723	1.1%	1.0%
33	501	730	1.0%	0.9%
34	505	737	0.8%	0.9%
35	510	744	1.0%	0.9%
36	515	751	1.0%	0.9%
37	519	757	0.8%	0.8%
38	523	763	0.8%	0.8%

Table 4.11 Tabulated surface area for 1 gram of pyrrhotite spheres over a range of diameters.

pyrrhotite diameter (mm)	SA_{sphere} (mm^2)	V_{sphere} (mm^3)	mass of particle (g)	# spheres in 1 gram	total surface area for 1 gram (mm^2)	Relative amount of surface area	SSA_{sphere}^* (mm^2/g)
0.001	3.14E-06	5.24E-10	2.41E-12	4.15E+11	1.30E+06	10,000	217,391
0.01	3.14E-04	5.24E-07	2.41E-09	4.15E+08	1.30E+05	1,000	21,739
0.1	3.14E-02	5.24E-04	2.41E-06	4.15E+05	1.30E+04	100	2,174
1	3.14E+00	5.24E-01	2.41E-03	4.15E+02	1.30E+03	10	217
10	3.14E+02	5.24E+02	2.41E+00	4.15E-01	1.30E+02	1	22

* Used a pyrrhotite density of $4.6 \text{ g}\cdot\text{cm}^{-3}$ ($0.0046 \text{ g}\cdot\text{mm}^{-3}$).

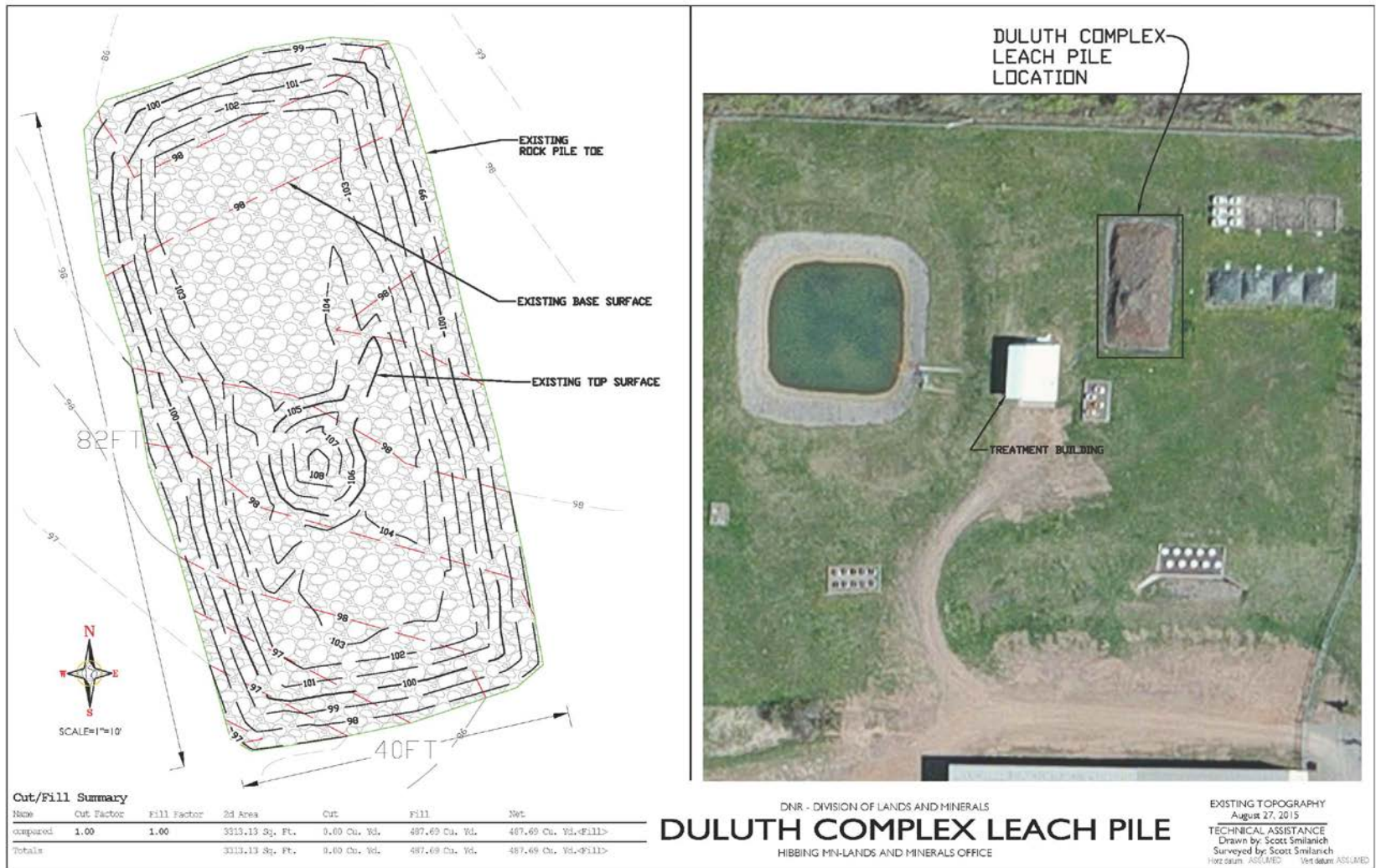


Figure 1.1 Surveyed topography of the DCLP and satellite image of the Hibbing field research site indicating the location of the DCLP.

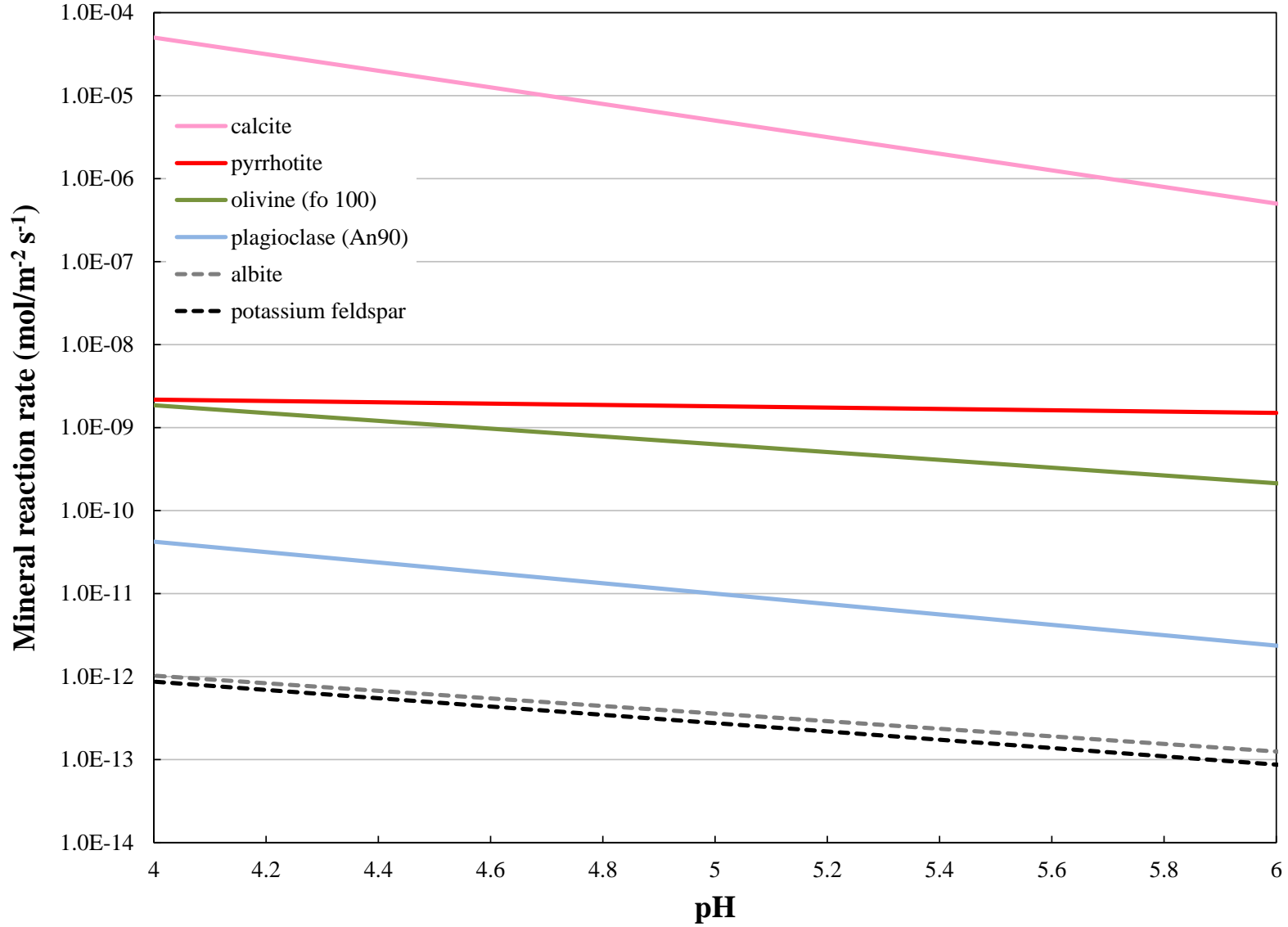


Figure 2.1 Mineral reaction rates as a function of pH (Palandri and Kharaka, 2004). For pyrrhotite an atmospheric equilibrated aqueous oxygen concentration was used (Bilenker et al., 2015).

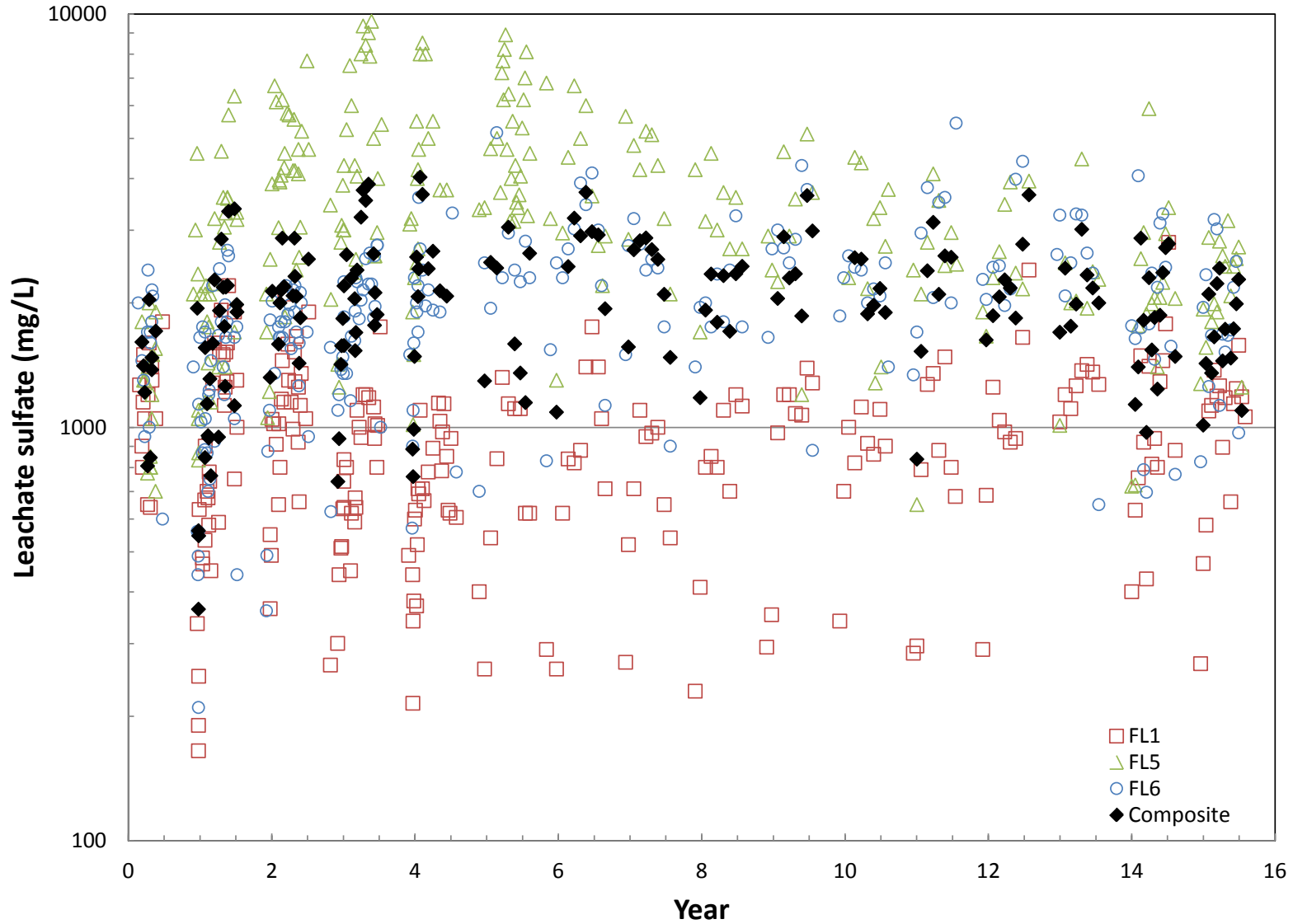


Figure 3.1 Leachate sulfate concentrations for the three former Amax field study rock piles and the calculated volume weighted composite values used in this study. The calculated values show good agreement based on what would be expected from bulk sulfur concentration of the DCLP.

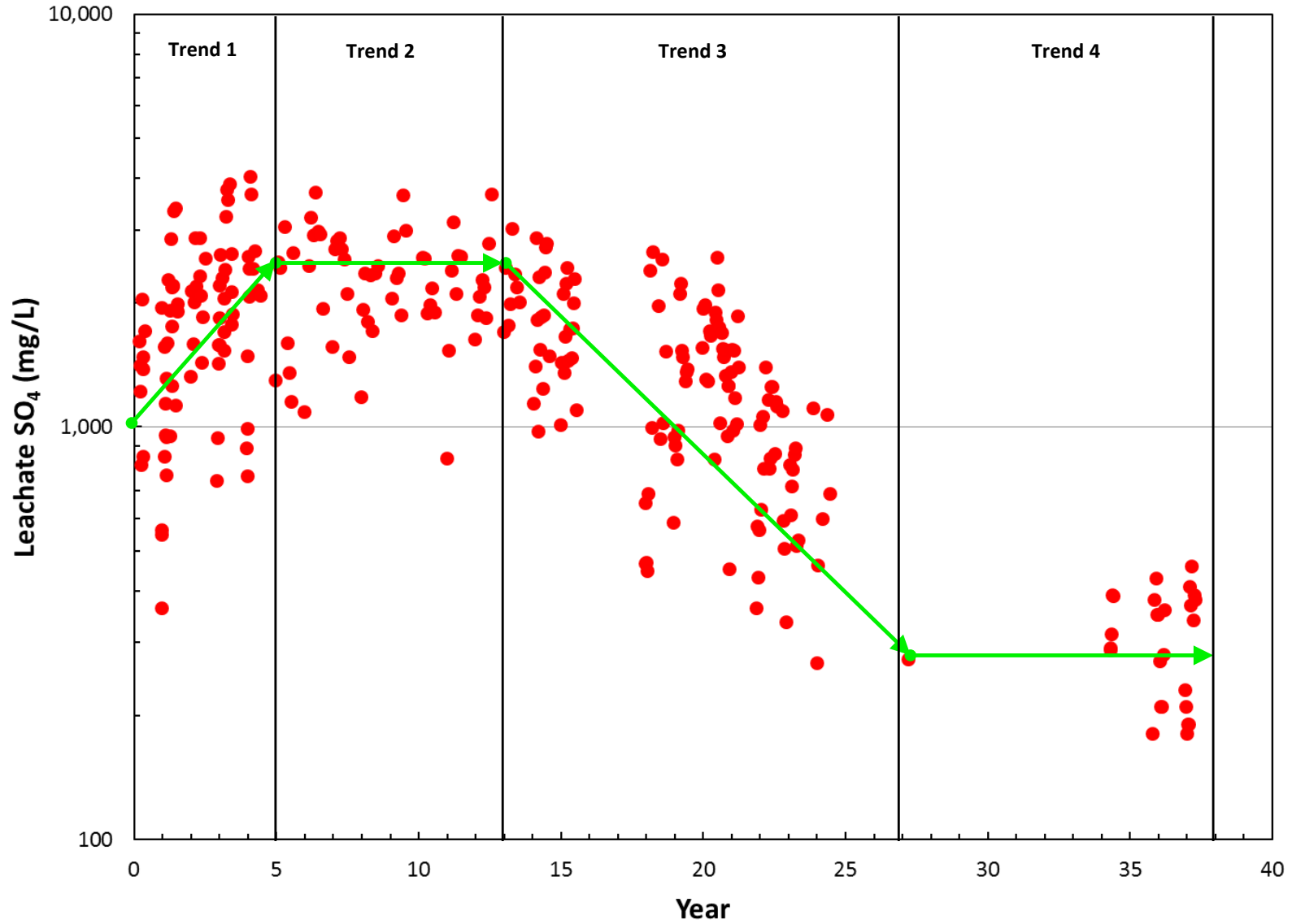


Figure 4.1 DCLP 38 year record of leachate sulfate concentration illustrating four principal concentration trends.

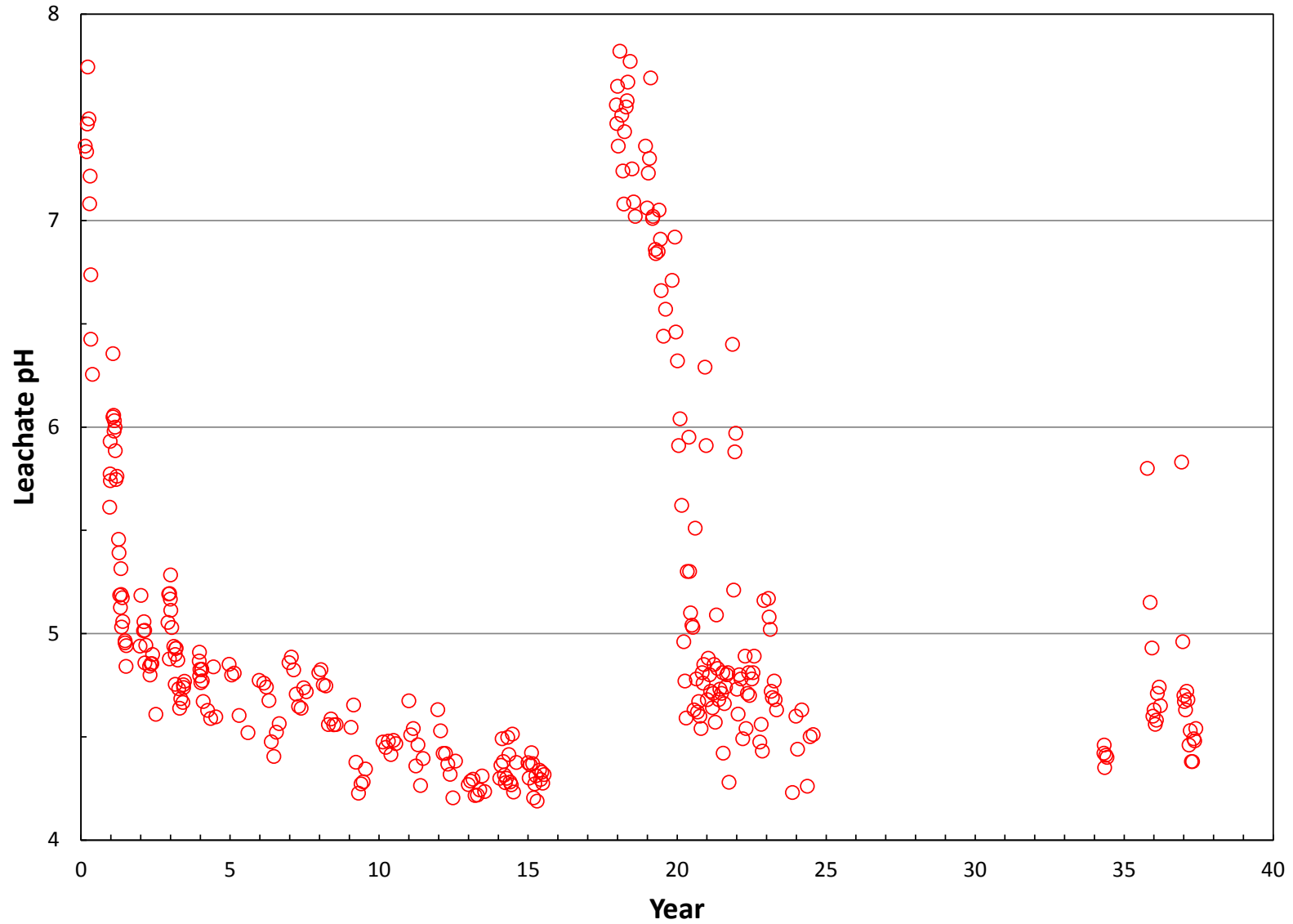


Figure 4.2 Leachate pH time series plot for the DCLP. Leachate pH at year 18 reflects the time at which the DCLP was placed at the Hibbing field research site.

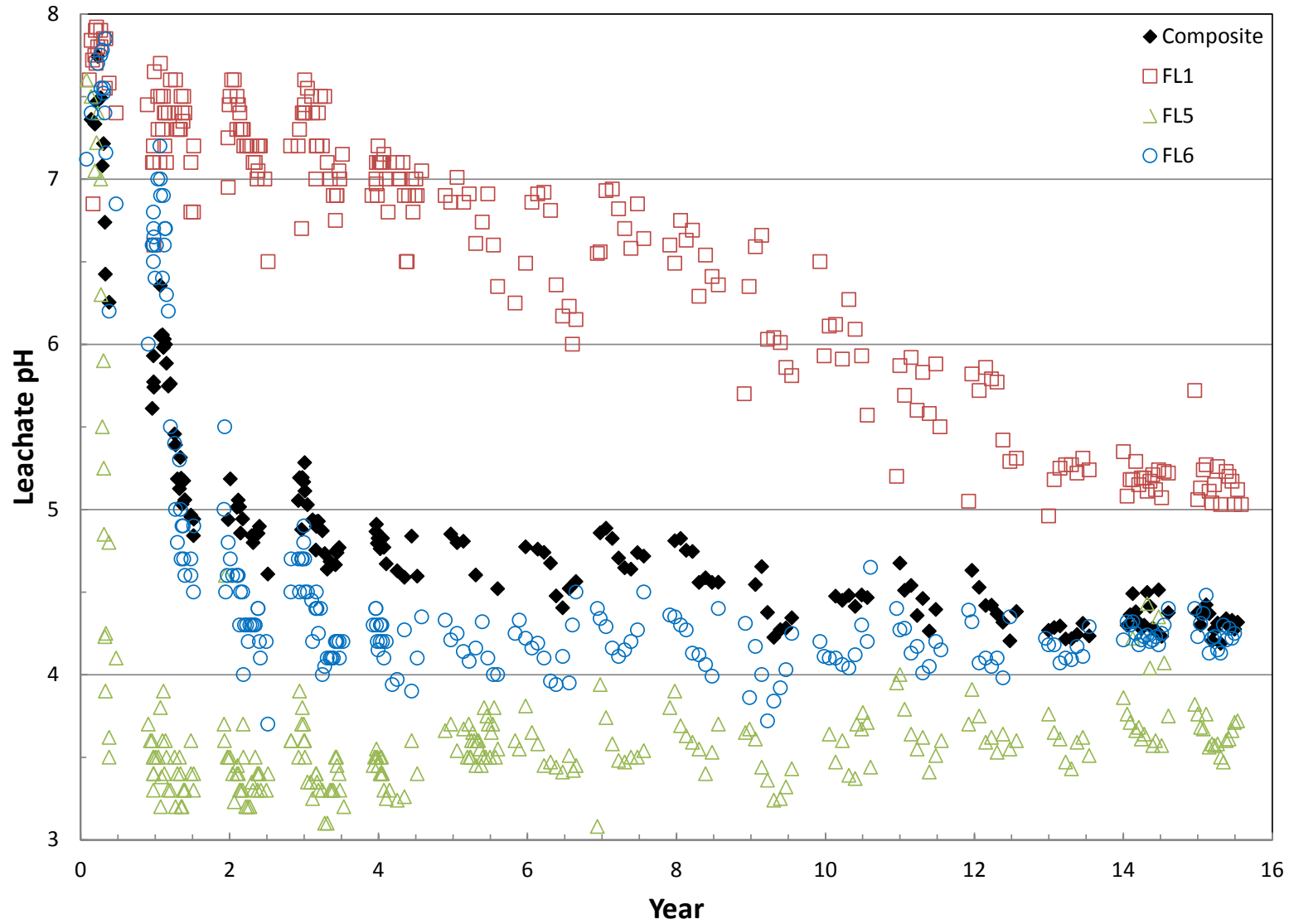


Figure 4.3 Leachate pH time series plot for the DCLP composite calculation and the three Amax field study rock piles the DCLP was calculated from.

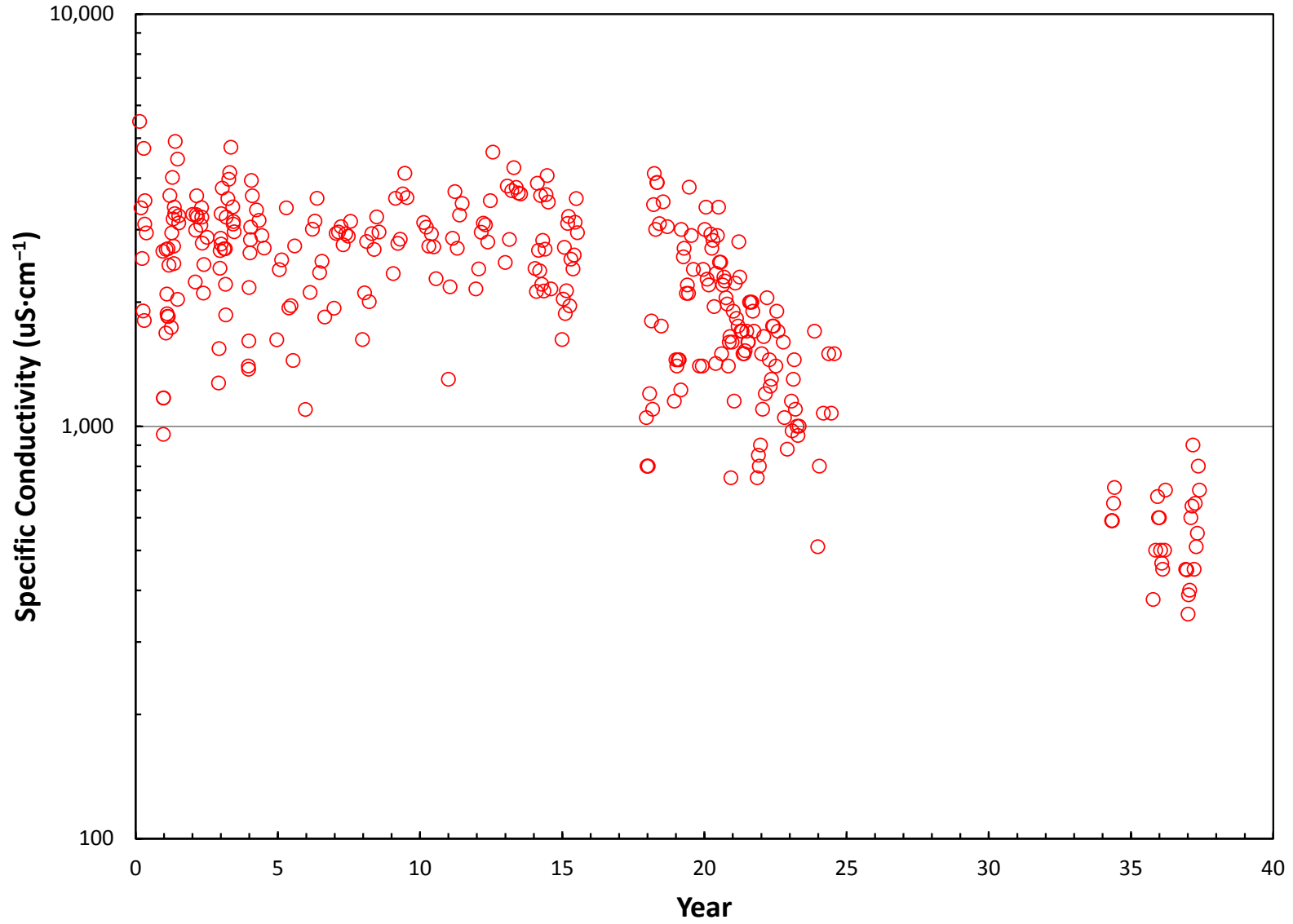


Figure 4.4 DCLP leachate specific conductivity time series plot.

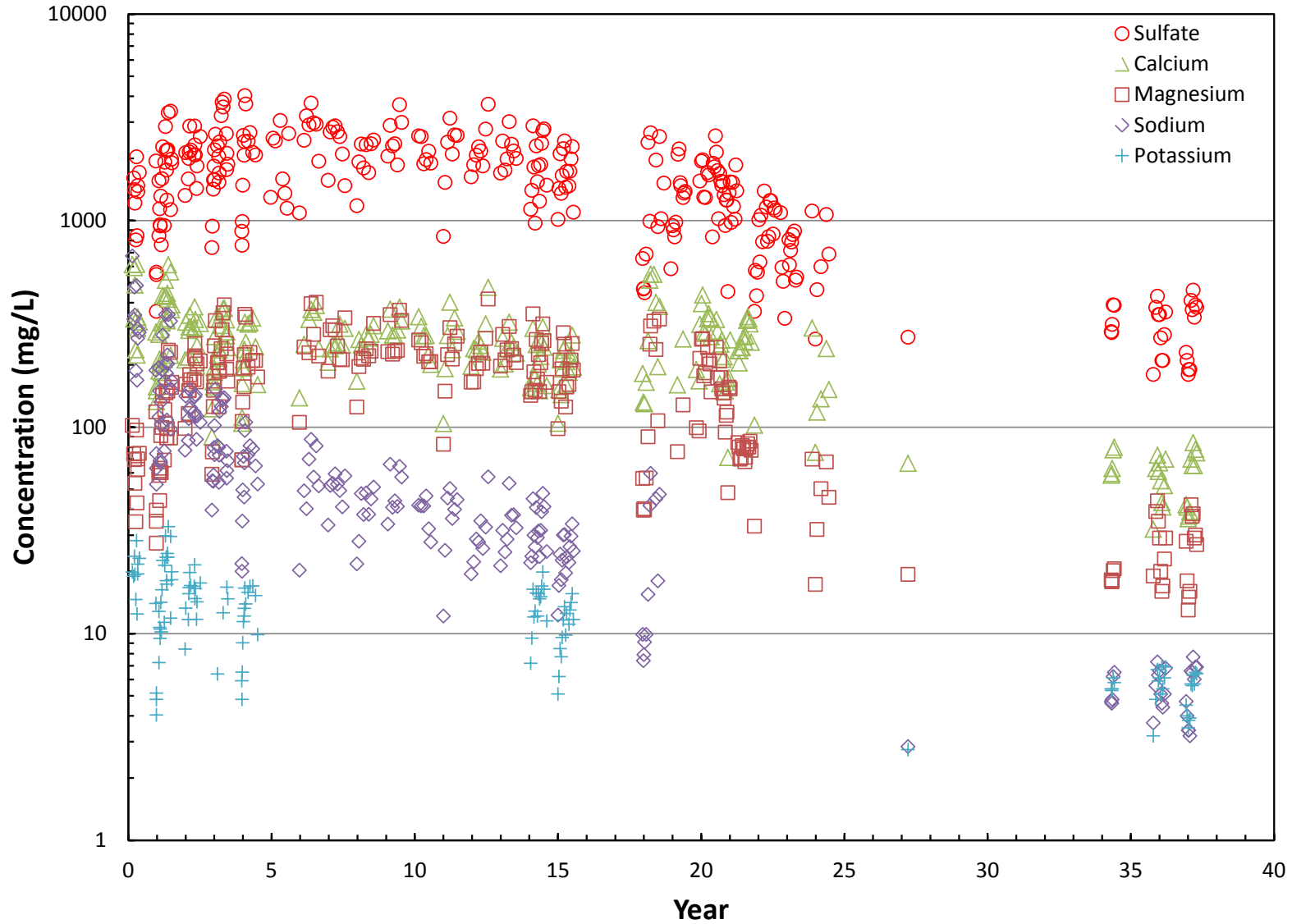


Figure 4.5 DCLP leachate sulfate and major cations concentrations time series plot.

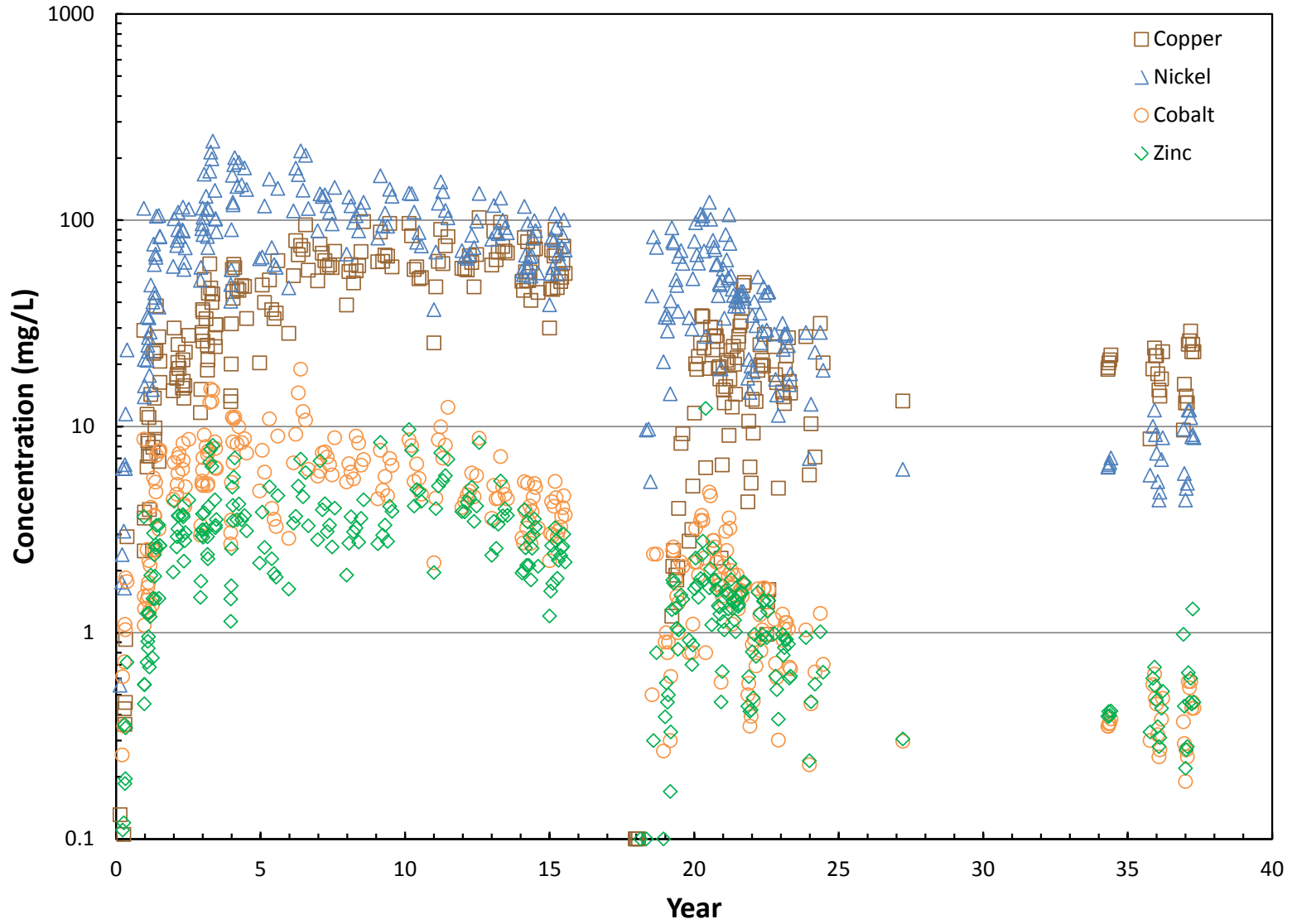


Figure 4.6 Select DCLP leachate metal concentrations time series plot.

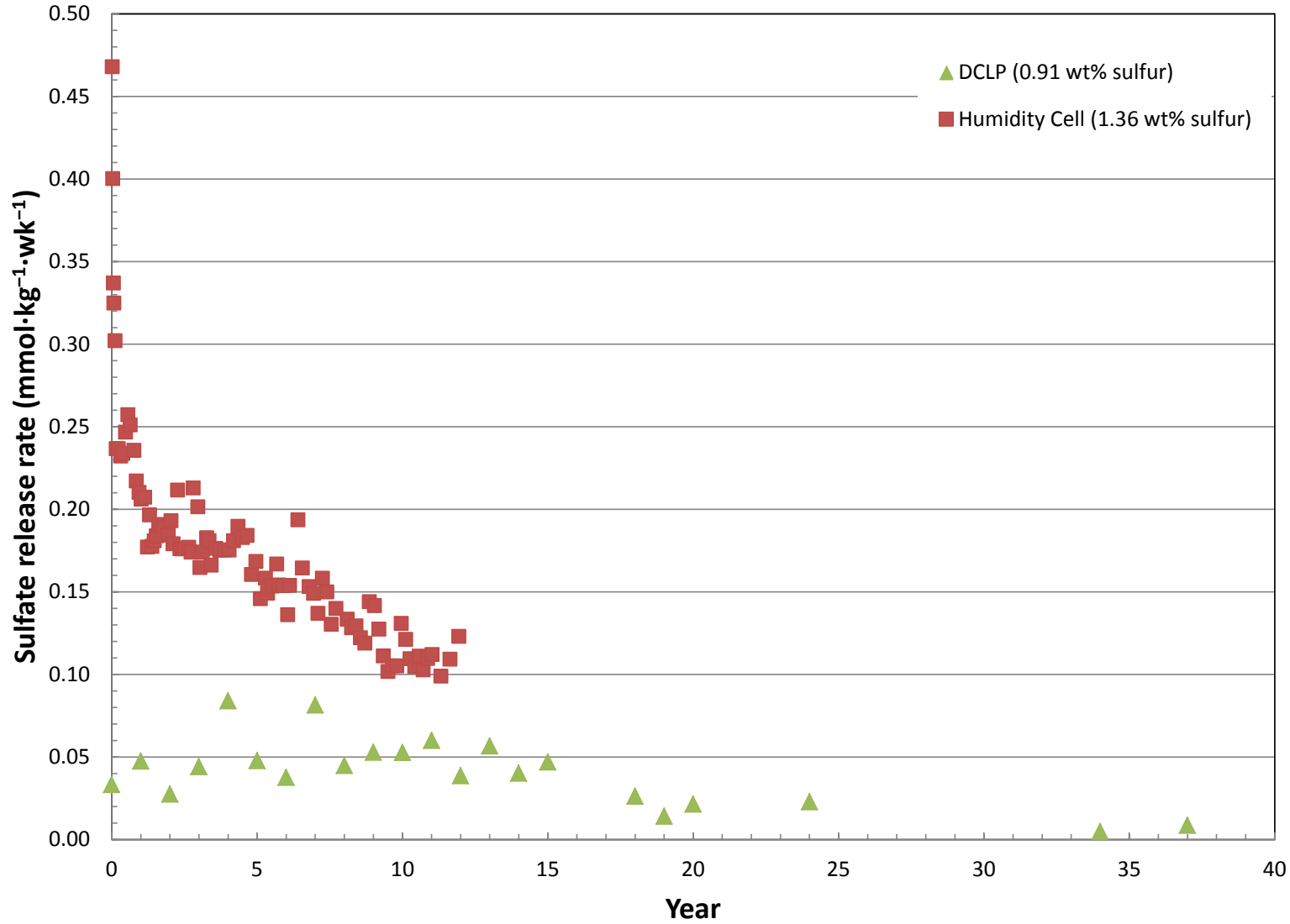


Figure 4.7 Sulfate release rate time series plot for leachate from the DCLP and a MN DNR Duluth Complex humidity cell. The humidity cell is number 16 from Lapakko et al. (2012).

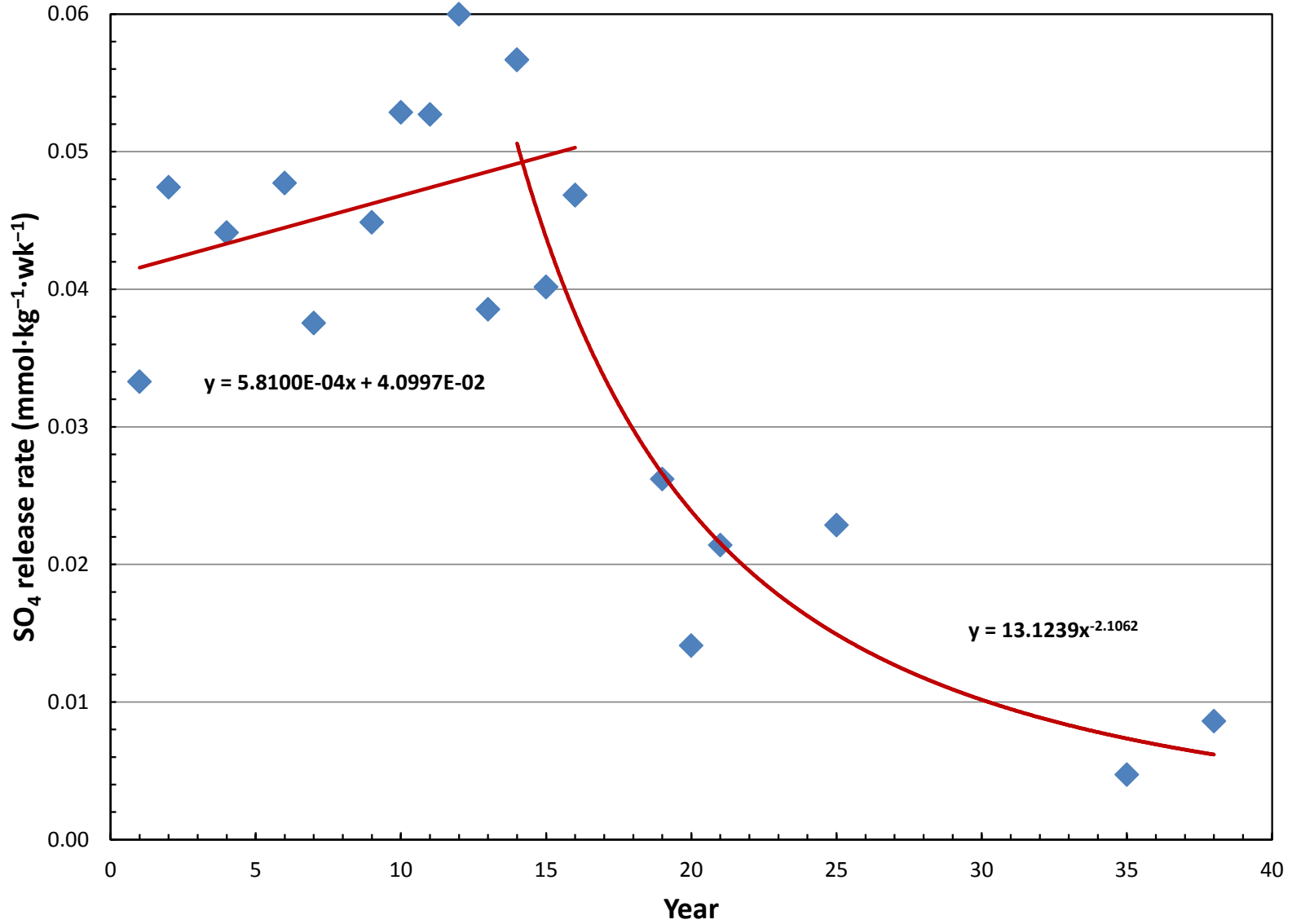


Figure 4.8 Empirical model of the linear and power function fit to the measured annual sulfate release rates. Sulfur removal was calculated using the equations of the lines for each regression.

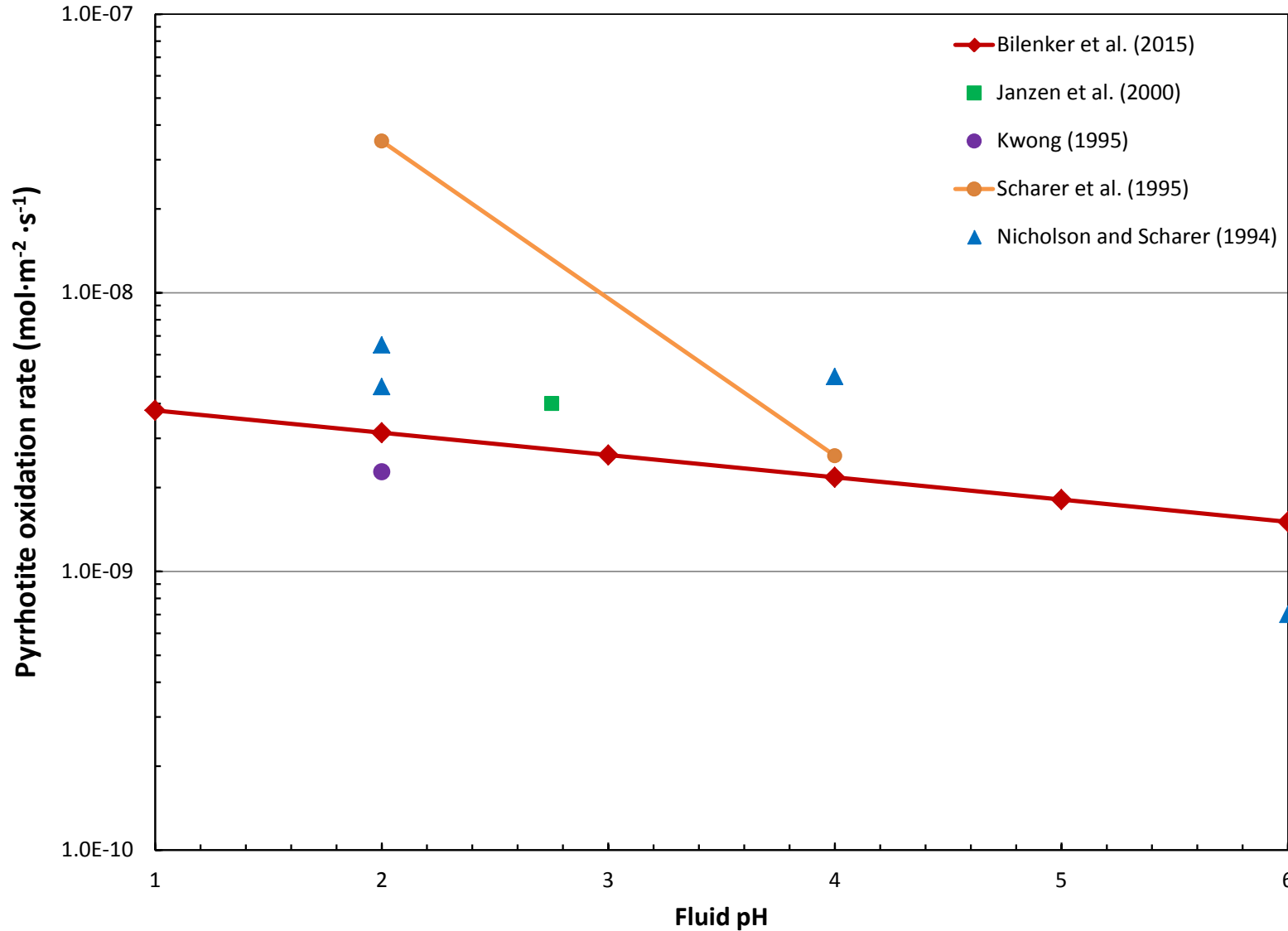


Figure 4.9 Surface area normalized pyrrhotite oxidation rates as a function of pH. The Bilenker et al. (2015) rate value was calculated using an atmospheric equilibrated oxygen concentration (2.648×10^{-4} molal). The Scharer et al. (1995) range spans a temperature range of 10 to 30° C.

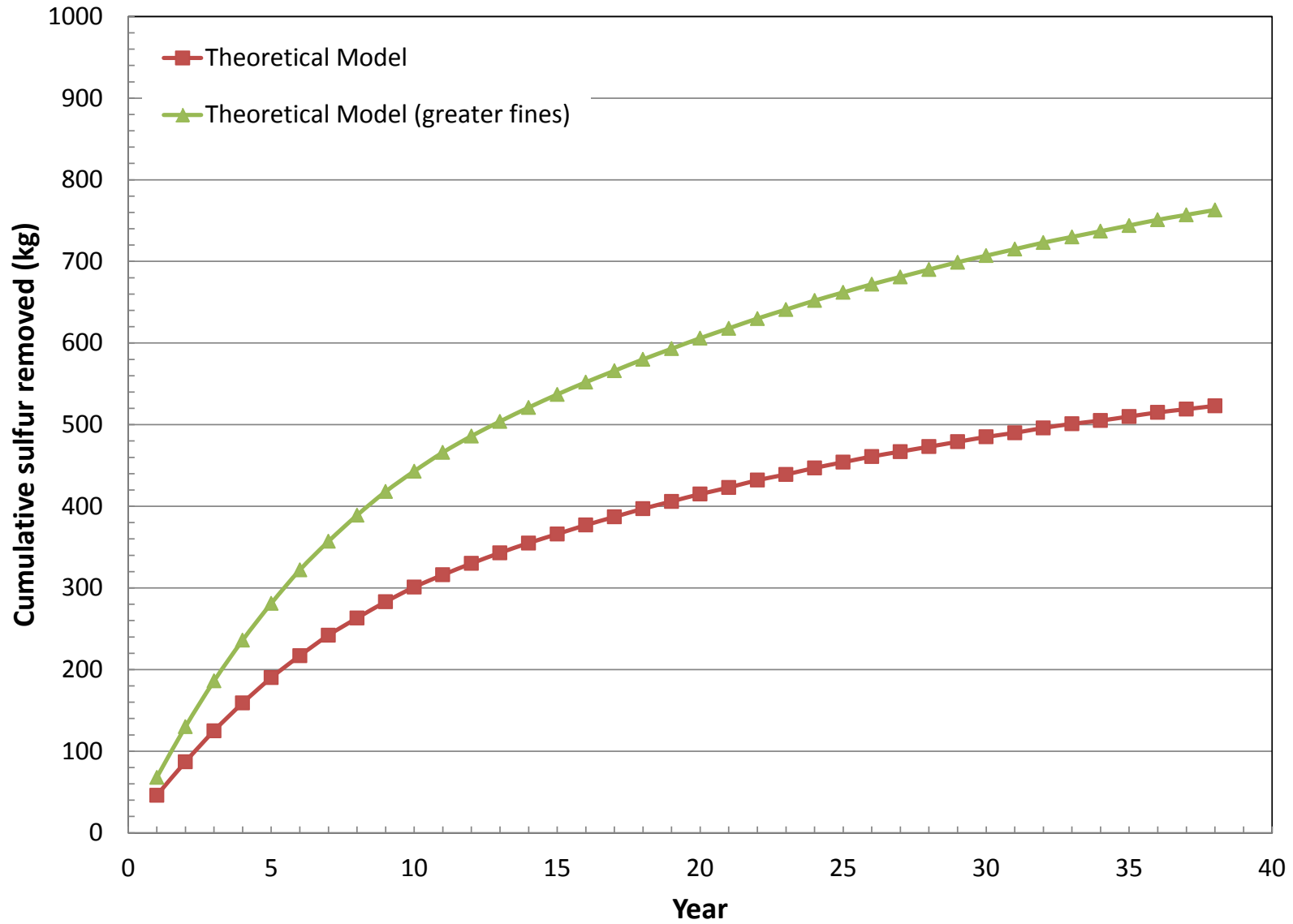


Figure 4.10 Theoretical model cumulative sulfur removal predictions for the normal and greater fines examples.

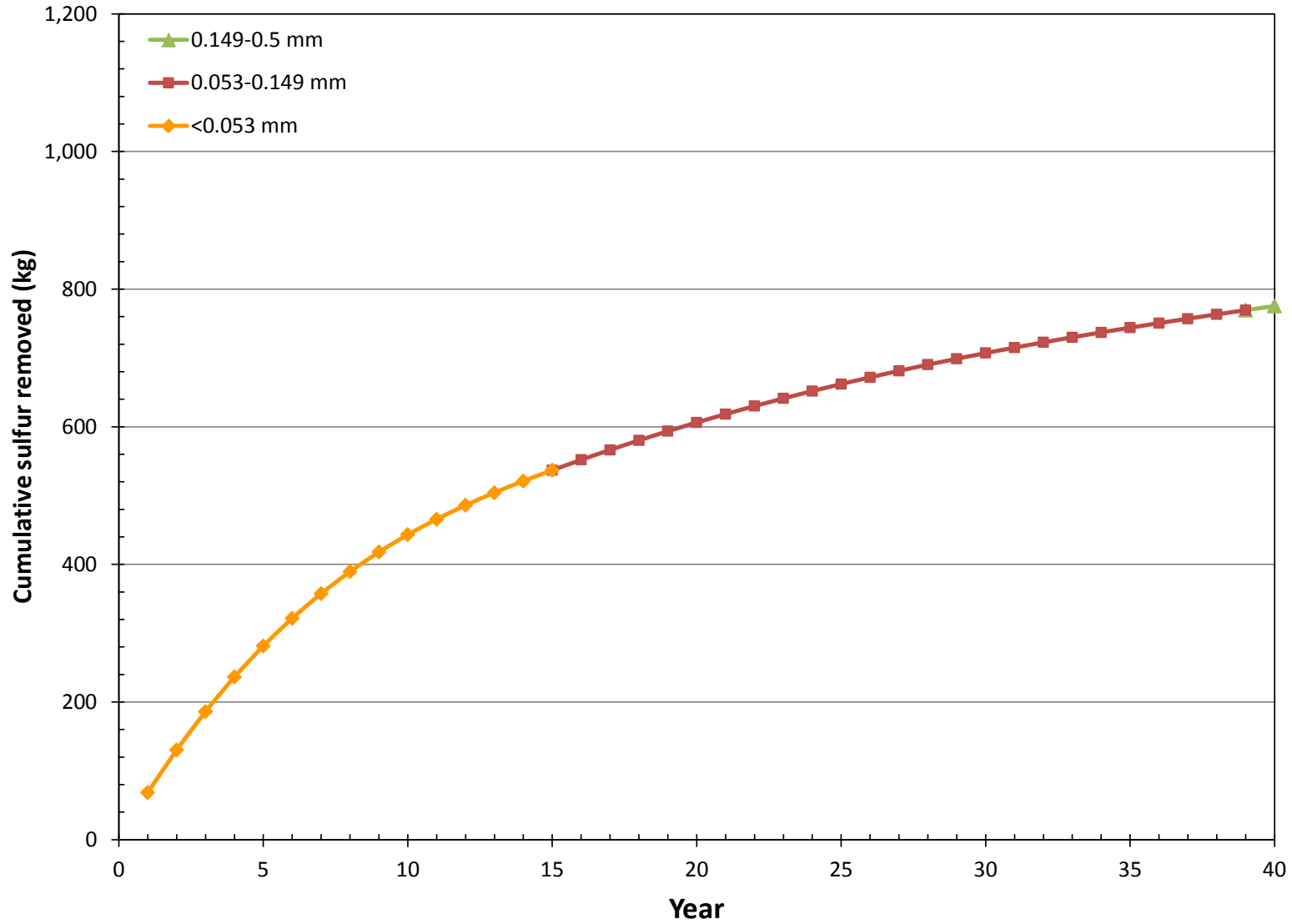


Figure 4.11 Cumulative sulfide removal of the greater fines example indicating the particle lifetime of the sulfide grains from specific rock particle size intervals.

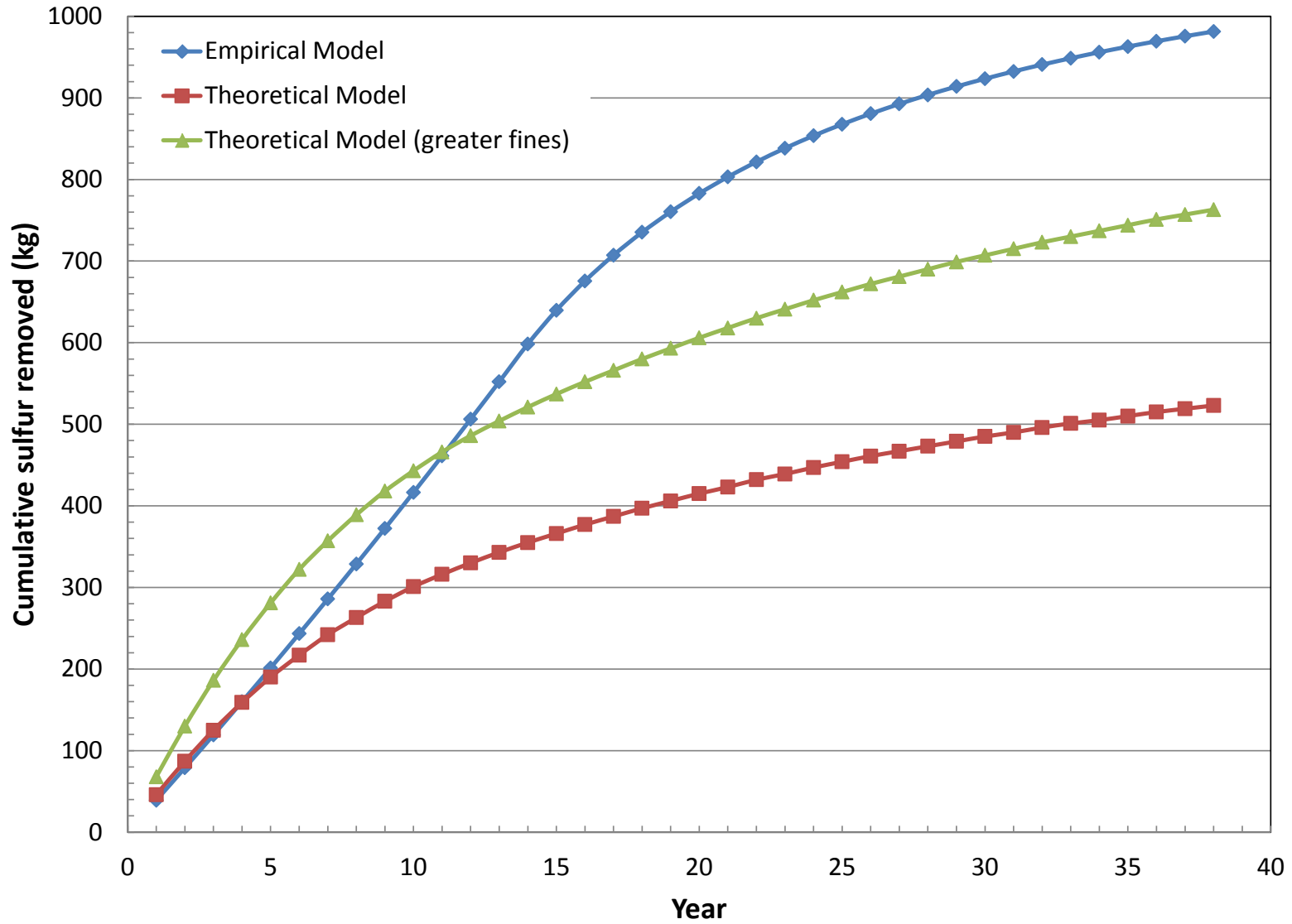


Figure 4.12 Cumulative sulfur removal plot for the empirical and theoretical models.

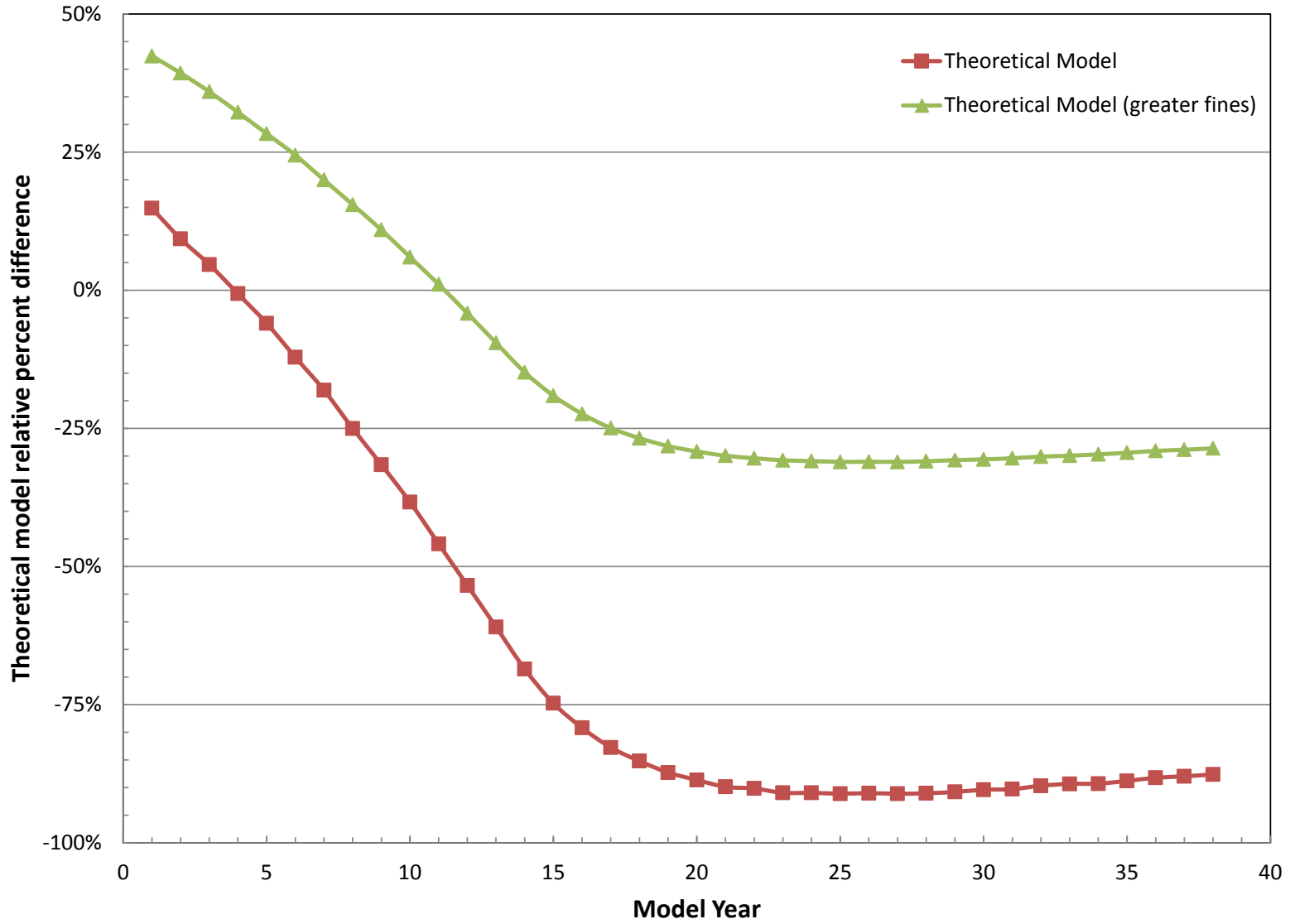


Figure 4.13 Relative percent difference of cumulative sulfur removal between the empirical model and the theoretical models.